The Search for Slow Moving Planets in the Distant Solar System.

by

Edward James Ashton

B.Sc. in Astronomy, University of Canterbury, New Zealand, 2012

A THESIS SUBMITTED IN PARTIAL FULFILLMENT OF
THE REQUIREMENTS FOR THE DEGREE OF

MASTER OF SCIENCE

in

The Faculty of Graduate and Postdoctoral Studies

(Astronomy)

THE UNIVERSITY OF BRITISH COLUMBIA

(Vancouver)

August 2017

Abstract

Out beyond the giant planets is a collection of bodies left over from planet formation. The objects that are just beyond Neptune are well studied compared to those that journey hundreds of au away; all such objects have been observed inside 100 au. We use a deep narrow survey and an uncommon technique to search for objects currently at large heliocentric distances. Using data from the Outer Solar System Origins Survey (OSSOS), which covered ~160 square degrees down to r $\sim$ 25, we searched for objects beyond 300 au. To find such objects we created a catalogue of all of the objects that were stationary of the astronomical seeing in three images taken over 2 hours. We then examined the stationary objects that were no longer there days/weeks/months before and after the three images. Although other astronomical phenomena like supernovae where discovered, no slow moving solar system object was found. From the null detection and using a survey simulator we obtain a 95% upper limit to the number of dwarf planets (-3 > H > 2) in the distant solar system, 1100^{+1700}_{-800}. To our knowledge this is the first published limit for dwarf planets beyond several hundred au.

Lay Summary

We searched a small fraction of the sky for slow moving solar system objects out at a distance rarely looked at. Since these objects were slow enough that they appeared to be stationary over a few hours, we used an algorithm to look for objects that were stationary in three images that were taken over two hours but moved on timescales more than a day. No such objects were found and that allowed us to estimate an upper limit on the number of dwarf planets in the distant solar system, 1100^{+1700}_{-800}.

Preface

All the images and catalogues, the validate software and the survey simulator were obtained from OSSOS with some parts altered by JJ Kavelaars to fit this work. The general idea for the technique used for finding slow moving solar system objects was the idea of my supervisor, Brett Gladman. I created the code described in Chapter 3, implementing the idea and dealing with unanticipated details. The results and analysis in Chapter 4 and 5 respectively are my original work.

Table of Contents

List of Tables

List of Figures

Acknowledgments

I would like to acknowledge my supervisor Brett Gladman for giving me the opportunity to work on research, for his guidance and discussions, and for being patient when the writing was slow.

JJ Kavelaars for creating the source catalogues for all of the nailing image, adding the RA and Dec coordinates to all catalogues and the couple of hours he futilely tried to get validate working on my laptop.

Lynne Jones and Simon Kurghoff for allowing me to join their team and for their helpful comments.

1. Introduction

1.1 Planet Formation

Planet formation is a complex process. We know that there is dust in protoplanetary disks due to the detection of infrared excess, and planets have been found around enough stars to say that planets are common phenomena in the galaxy. What is not known is in what way does dust come together to form planets.

Currently there are a few theories on how planets come to be. One such theory follows the idea that planets formed the same way as stars, by gravitational collapse, where most of the gas and dust in a region of the protoplanetary disk collapses to form a planet (Boss, 1997). This could be how the giant planets formed, although the metal abundence in Jupiter's atmosphere is higher than that of the sun (Young et al., 1996), which should not be the case if Jupiter was formed by gravitational collapse. The discrepancy in metal abundance could be remedied by Jupiter being polluted by rocky objects. Gravitational collapse or 'local instability' is thus less favoured for the formation of giant planets in the Solar System.

The leading theory of planet formation is known as 'bottom up accretion' or core accretion. This is where particles collide forming a collection of objects that slowly increase in average mass until the most massive objects become planets. To form the gas envelopes around the giant planets, once the most massive objects were big enough they were able to accrete gas (Lissauer et al., 2009). Bottom up accretion, too, has problems. In protoplanetary disks the pressure gradient causes gas to orbit at sub-keplerian speeds. The solid objects, which travel at the keplerian rate, will therefore feel a gas drag and drift towards the star. This drift has the highest effect on metre sized objects, since smaller objects are coupled to the gas and larger objects have a small surface area to mass ratio. Therefore metre sized objects have to grow quickly or else they will spiral into the star, a metre sized object at 10 au has a lifetime of approximately a thousand years. This is known as the metre-size barrier (Weidenschilling, 1977). A way around the metre barrier is to have the dust clump into kilometre sized objects, known as planetesimals, on a shorter timescale and then grow by colliding into one another.

A problem with bottom up accretion is simulations suggests the time taken to form planets may be too long. A way to speed up accretion is to have 'pebble' sized objects ($\sim$cm scale) accrete onto planetesimals when they get to 100s of kilometres in diameter. In this regime the size of the planetesimals collection area results in a high accretion rate (Lambrechts and Johansen, 2012). This theory, known as pebble accretion, can form planets in a timescale that agrees with observations. It is plausible that there is not just one planet formation mechanism but multiple process depending on the environment.

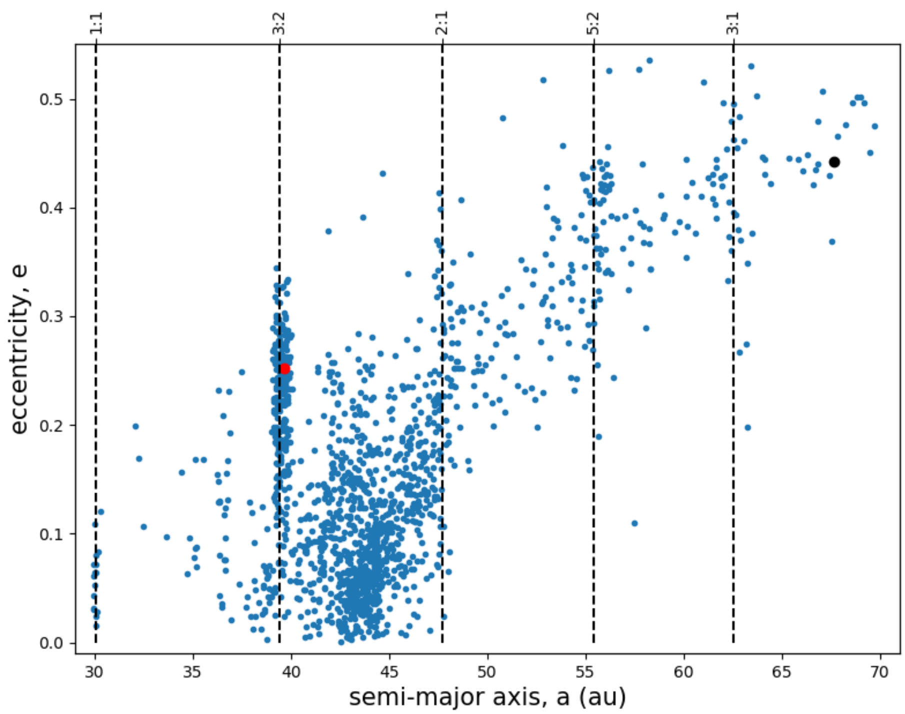

Figure 1.1: Known TNOs that have a pericentre greater than 25 au. The semi-major axis that correspond to certain MMR are given as dashed lines. The two largest TNOs have been coloured differently with Pluto in red and Eris in Black. Data obtained from the Minor Planet Center and are osculating heliocentric orbits.

1.2 The Structure of the Outer Solar System

Whatever the mechanism of planet formation, there are planets and minor bodies, both in the Solar System and in other stellar system. The outer Solar System (Jupiter and beyond) contains four giant planets[1], and a size distribution of smaller objects up to $\sim$1000 km in radius. Almost all of these smaller objects have semi-major axis beyond that of Neptune. These objects are known as Trans-Neptunian Objects (TNOs).

There is a swarm of icy debris just outside the orbit of Neptune known as the Kuiper Belt analogous to the asteroid belt. The Kuiper belt objects (KBOs) can be split up into resonant and non-resonant. The resonant KBOs have periods that are near integer ratios of the period of Neptune. The time it takes for a resonant KBO to complete N integer orbits is the same as the time Neptune takes to complete M integer orbits. This phenomena is known as mean motion resonance (MMR). Non-resonant KBOs are simply those that are not in MMR with Neptune. There might be another separation in KBOs. There is evidence of two different inclination distributions in the Kuiper Belt. The distribution of objects that have, on average, lower inclinations ($\sim 3^\circ$) are known as cold KBOs. Similarly the higher inclination distribution ($>5^\circ$) objects are

[1]There might have been a fifth giant planet in the giant planet region in the past that had a close encounter with one of the other giant planets and was ejected from the Solar System (Nesvorný, 2011).

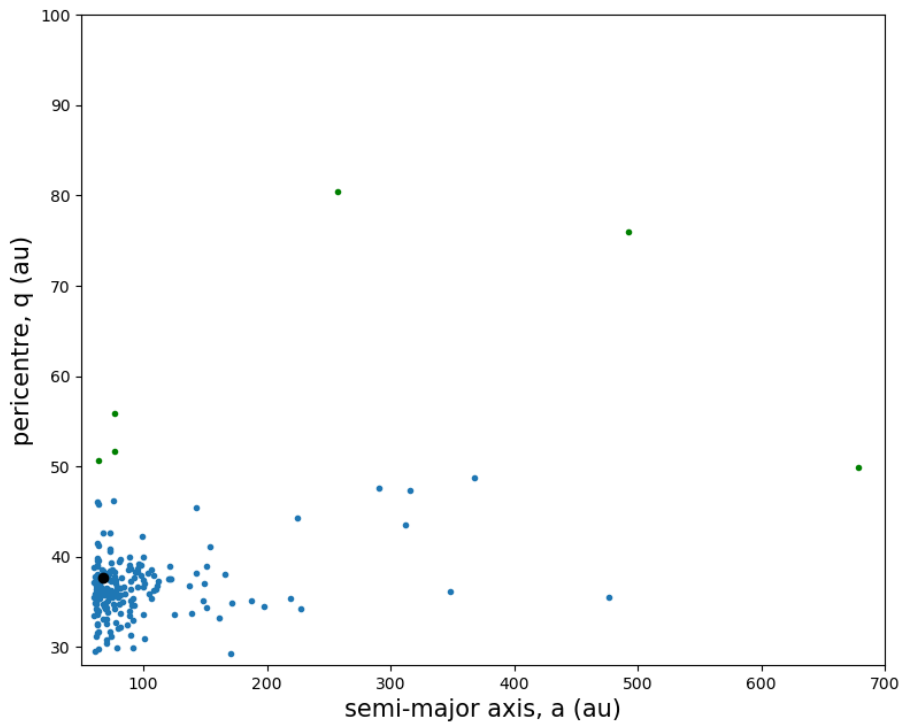

Figure 1.2: All (but one) of the known TNOs that have semi-major axes greater than 65 au and a pericentres greater than 29 au. The missing object is 2014 FE72, with a semi-major axis of 2055 au, far greater than the next highest. Eris, with a = 67.6 au, has been coloured black. Data obtained from the Minor Planet Center and are osculating heliocentric orbits.

known as hot KBOs(Brown, 2001). An observation that supports this (dynamical) division is that cold KBOs have, on average, redder optical colours than hot KBOs. The non-resonant Kuiper Belt is made up of hot and cold KBOs, whereas the resonant appear to be all hot KBOs.

The close proximity of Neptune to the Kuiper belt results in gravitational interactions between Neptune and KBOs but the dynamical lifetimes of KBOs are gigayears. There is a population of objects that have dynamical stability timescales that are much less that KBOs known as the scattering objects (SOs). Named as they are readily scattering off Neptune, and as such usually have high eccentricities and pericentre near Neptune's orbit. If a SO is scattered to a semi-major axis less than that of Neptune then the object is called a Centaur.

There are TNOs that are no longer interacting with Neptune. If a TNO's pericenter is greater than about 37 au. and it is not in a MMR with Neptune, it is said to be detached from Neptune and are thus named Detached Objects (Dos). They are believed to be SOs at one point in time and, after an interaction with another body, had their pericenters raised.

Far beyond the Kuiper Belt is the theorised Oort Cloud, which is the reservoir of isotropic comets that have near parabolic orbits. The Oort cloud consists of an inner and outer region. The inner Oort cloud, which starts about 2,000 au, is more of a disk shape. Whereas the outer Oort cloud is nearly spherical, and it might extend out to hundreds of thousands of au.

The TNOs that have been discovered so far are shown in Figure 1.1. The grouping of the resonant Kuiper Belt around MMR can be clearly seen with the 3:2 (3 Neptune orbits for 2 of the KBOs orbits) being the most populated. Also seen is a large grouping of TNOs between the 3:2 and 2:1 MMR populations, this is where the vast majority of the cold KBOs lie. Out beyond 50 au there is a trend of increased eccentricity with increased semi-major axis. These objects are mostly SOs or DOs.

Known TNOs with high semi-major axis, where almost all are SOs and DOs, are shown in Figure 1.2. The only TNO which has a semi-major axis greater than 65 and is not Neptune crossing that is not shown in the figure is 2014 FE72, with a semi-major axis of 2055 au and pericentre of 36 au. Due to its incredibly large semi-major axis and the fact its not Neptune cross, 2014 FE72 could be the first inner Oort cloud object discovered. No outer Oort cloud object with a pericentre beyond Neptune has been found yet.

The higher the semi-major axis is, the further away a TNO generally is from the Earth, the fainter it is. Therefore we are biased towards objects with low semi-major axis. Looking at the high semi-major axis (a>150 au) TNOs in Figure 1.2 the bias is clearly evident, the higher the semi-major axis, the less detected TNOs there are. Simulatoins suggest the real distribution of high semi-major axis TNO might be uniform(Lawler et al., 2017). Similarly the higher the pericentre is, the further away a TNO generally is from the Earth, the fainter it is. Therefore there is a bias towards objects with low pericentres, and again this can be seen in Figure 1.2.

So far, the largest TNOs found are Pluto sized. There are three of these objects; Pluto, Eris and Triton. Triton, which is now a moon of Neptune, is believed to have been part of the Kuiper Belt due to its retrograde orbit around Neptune. The main theorised capture method is Triton used to be part of a binary system with another KBO before they came too close to Neptune and Triton's companion was exchanged for Neptune (Agnor and Hamilton, 2006). Both Eris and Pluto are plausibly formed closer to the Sun and then planted into their current hot-population detached and 3:2 resonant orbits respectively.

1.3 The Origin of TNOs

TNOs are believed to be left over planetesimals from planet formation, although there could be some collisional evolution since then. The cores of the giant planets are significantly more massive compared to the largest TNO ($\sim 10 M_e$ compared to $0.02 M_e$), so the giant planet cores were likely formed by runaway accretion. Runaway accretion happens when the larger planetary embryos that became the giant planets were able to accrete at a much faster rate than the rest of the smaller planetesimals. This results in a few discreet outliers (Giant planets) and a continuous distribution of smaller objects (TNOs).

During planet formation, when the giant planets were massive enough, they were able to kick out all of the remaining planetesimals from the giant planet region. Most of the planetesimals were ejected from the Solar System but small fraction were relocated to the Kuiper belt, scattered disk and Oort cloud. Most of the retained planetesimals are in the Oort cloud with the Kuiper Belt receiving the least, perhaps ∼0.1%. This ejection event caused accretion of planetesimals in the outer solar system to cease, and along with the infrequency of collisions due to low number density, resulted in the size distribution of planetesimals 'freezing out'. Therefore the size distribution of objects in the Kuiper belt and scattered disk today is the same as the size distribution of planetesimals in the early Solar System.

1.3.1 Effects of an Extra Planet

If Batygin and Brown (2016) are correct in their prediction of a $10M_E$ planet with a ∼600 au, then this extra planet will effect the dynamics of the SOs. This prophesied ninth planet would affect the number of scattered objects that are ejected, and modify the current orbital distribution in the a = 200 - 1000 au range(Lawler et al., 2017).

1.4 Undiscovered TNOs

In terms of searching for another giant planet, NASA's Wide-Field Infrared Survey Explorer (WISE) space telescope has search the sky in the infrared for distant objects in the Solar System. WISE has ruled out a Saturn sized object or larger out to 28,000 au and a Jupiter sized object or larger to 82,000 au (Luhman, 2014).

If there was another Pluto sized object in the Solar System where could it be? Another object that lies in the planet region would have been discovered by now. If the object was within a couple of hundred au it had a ∼66% chance of being found by the Schwamb et al. (2009) search of the ecliptic, unless it was highly inclined or in the galactic plane. That leaves out beyond a couple of hundred au. If any Pluto sized object is out there they would likely be a SO or DO near apocentre of a large eccentricity orbit.

If 100-1000 Pluto sized objects were formed initially, then 10s could still remain in KB and SD today. So there could be enough large objects in the scattered disk to warrant a search beyond a few 100 au.

1.4.1 TNO survey limits

The major problem with detecting objects out beyond a ∼200 au is the amount of light received from them. The flux from an object drops off as the distance squared but since the light from bodies in the Solar System is reflected sunlight there is another factor of distance squared, resulting in the flux of a distant solar system object being proportional to $1/d^4$. This means distant TNOs are incredibly faint. If Pluto was moved from where it currently is at 30 au out to 300 au, the increase in distance by a factor of 10 would result in a decrease in flux by a factor of 10,000, corresponding to a change in magnitude of 10, dropping it from ∼14th to ∼24th magnitude, fainter than the flux limits of the very large-field surveys (the Schwamb et al. (2009) limit was mag 21).

Another, but not as severe, problem is the on-sky motion of distant objects. Objects in the Kuiper Belt and beyond are far enough away that their on-sky motion is dominated by the

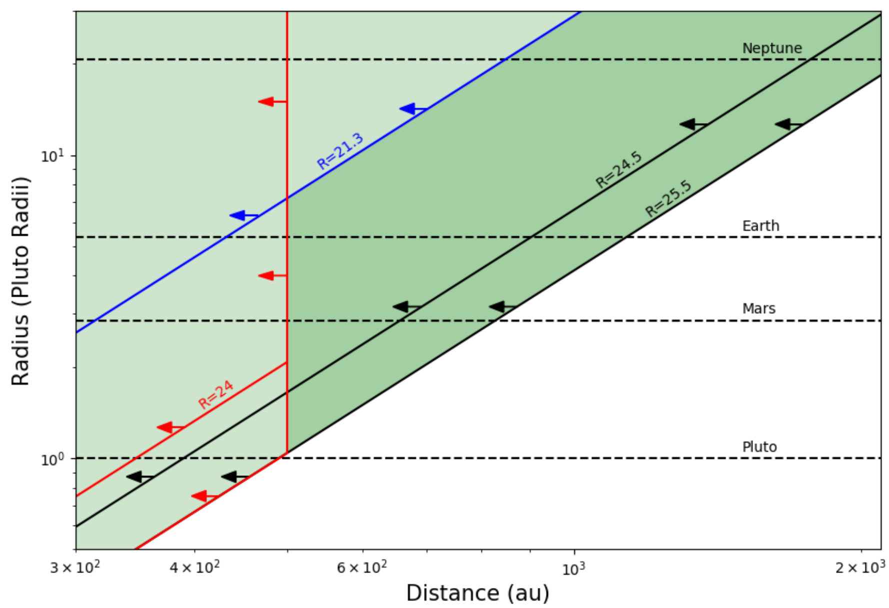

Figure 1.3: A comparison of how far, for a certain sized object, three surveys could detect out to. The three surveys Schwamb and Brown (blue), Sheppard and Trujillo (red), and this work (black). The solid lines represent the limit of the region of phase space which an object can be detected by the surveys. The diagonal lines are caused by the limiting R band magnitude, these values are displayed above each line and were created by scaling Pluto apparent magnitude. The shaded green area is the region of phase space that this work is sensitive to, with dark green only this work and light green if there is overlap with other surveys.

Earths orbital velocity. Therefore a TNO at opposition would have a retrograde on sky-velocity, in arcseconds per hour, approximated by

$$rate = \frac{150}{d} \quad ''/hour \tag{1.1}$$

where d is the object's heliocentric distance in au. The further away an object the slower its sky motion. Conventional KPO surveys have ≈1 hour cadences that are optimal for KPO speeds, therefore usually are only able to detect objects within a ∼300 au.

1.4.2 Distant TNO Surveys

At the beginning of this work, the only known survey that could search for distant Pluto-sized TNOs was the Schwamb et al. (2009) survey, which will be referred to as Schwamb and Brown. They covered a sky area of ∼12,000 square degrees and stated that they were able to detect objects out to 1000 au, which was achieved by having a multi night discovery baseline. Their stated limiting magnitude is R = 21.3, this corresponds to Pluto at 165 au.

After this project started a paper detailing another TNO survey was release. Sheppard and Trujillo (2016), which will be referred to as Sheppard and Trujillo, searched a thousand squared degrees and, according to the paper, could detect motion down to 0.3 arcseconds per hour. Using Eq. 1.1, that speed corresponds to an object at 500 au. This survey used multiple telescopes so there is a large range of limiting magnitudes. A majority of the images were taken with Chile where the limiting magnitude ranges from about 24 to 24.6. Less than 10% of the Survey was taken with Magellan and Subaru telescopes, where the limit magnitude went down to ∼25.5.

For a better understanding of the limits of these two surveys, the distance to an object, of a particular size, that each survey can detect out to is plotted in Figure 1.3. The region which this work covers is also plotted. In regards to detecting Pluto sized objects at these distances, Schwamb and Brown are not sensitive enough (they could only just see Mars sized objects at 300 au). Sheppard and Trujillo, on the other hand, are able to see Pluto sized objects out to almost 500 au, only for a small fraction of survey. Most of the survey could not see objects fainter than 24.6, which is Pluto at ∼350 au. It should also be noted that almost all of the sky patches that Sheppard and Trujillo observed are below the ecliptic and therefore do not overlap with the area observed for this work.

1.4.3 Improving Surveys

There are two ways a survey can increase the number of discovered objects, increase the sky coverage or increase the depth of the images. If the sky has uniform surface density of objects (for TNOs near the ecliptic this is approximately true) then one would expect the fractional increase in sky coverage to be the same as the fractional increase in detected objects. It is a little more complicated for the case of increasing the image depth, for it depends on the absolute H magnitude distribution[2]. If the slope of the H mag distribution of objects that are just too

[2] H magnitude is defined as the magnitude of an object if it was 1 au away from both the Sun and Earth and it is was at opposition

faint to be detected was shallow there would be little justification for increasing the depth. The cumulative H mag distribution appears to obey the following

$$\frac{dN(<H)}{dH} \propto 10^{\alpha H} \tag{1.2}$$

where N(<H) is the number of object that have a H mag of 'H' or less and α is logarithmic slope. The cumulative H mag distribution for the brightest TNOs is shown in Figure 1.4. There appears to be two different slopes. The size distribution is shallower at lower H, with $\alpha \sim 0.14$, and steeper at higher H, with $\alpha \sim 0.6$. The knee between the two slopes is at H $\sim$ 3. This is an incomplete sample of bright TNO. It is believed that there are few more undiscovered brighter than H $\sim$ 3 within a couple of hundred au. Therefore the slope of the real distribution might be slightly different to the current slope but two distinct slopes is believed to be a real feature. A clear sign of the incompleteness is the fact that at H $\sim$ 6 the slope slowly shallows off. At around H = -0.5 the data diverges from the trend, this is due to low number statistics, there are only two objects brighter than -0.5.

At 300 au a TNO that has an apparent magnitude 25.5 will have an H magnitude of about 1.4. Since this TNO would be the smallest object these surveys could find, at distances beyond 300 au, we only have to worry about the shallow region of the H mag distribution. Therefore an increase in limiting magnitude would not produce a large increase in objects found, or in this case not significantly increase the chance of finding an object. This means this survey is not ideal for finding distant objects. A survey with a larger sky coverage and a magnitude shallower would have a better chance of finding a distant object. Although this survey is probing a unique region of parameter space.

1.5 Thesis Outline

The structure of the rest of this thesis is as follows; information about the survey used in this work is detailed in Chapter 2. Chapter 3 explains the way we searched the data set for slow moving object, including the algorithm that aided us. We detail the findings of the search in Chapter 4. The upper limit for Dwarf planets and how it was obtained can be found in Chapter 5. Finally, we give concluding remarks in Chapter 6.

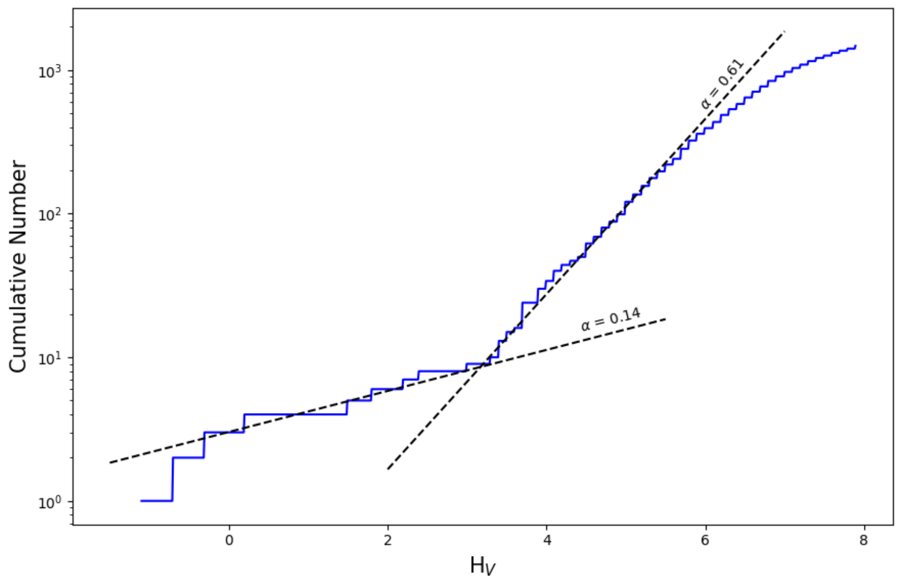

Figure 1.4: The cumulative distribution of the known TNOs down to a heliocentric absolute visual magnitude of 8 (blue line). Two exponential functions are plotted (dashed lines) to match the slope of the data. The logarithmic slope, α, of each exponential function is displayed above each line. The rollover beyond H $\sim$ 6 is likely the increasing observational incompleteness. Note: these are not lines of best fit for the data. Data obtained from the Minor Planets Center.

2. OSSOS

The data used for the search for the slow moving Solar System objects comes from the Outer Solar System Origins Survey (OSSOS). The original goal of OSSOS was to discover TNOs using the common method of searching for objects that move linearly in 3 images taken with 1-hour spacings, which allows detection out to about 300 au. Once found, these objects were then all tracked over months to years to measure their orbital elements with high precision. From 2013 to 2016 the images that makes up OSSOS was acquired using the Canadian France Hawaiian Telescope (CFHT), a 3.6 m telescope at Mauna Kea. For a more complete understanding of OSSOS please refer to Bannister et al. (2016).

The most distant OSSOS detection was found at a distance of 83 au (although there are 33 OSSOS TNOs with a ¿ 83 au whose orbits taken them out well beyond 200 au; with four having apocentre, Q=a(1+e), greater than 500 au. These large-a detections are discussed in Shankman et al. (2017).

OSSOS images were captured using MegaCam, a wide-field optical mosaic camera. Initially, MegaCam was able to capture 0.9 square degrees of sky area in one image using 36 charge couple devices (CCDs). Even though MegaCam was installed will 40 CCDs, with a total sky area of one square degree, the filter that was used at the time meant two CCDs on each side, known as the 'ears', could not be used. See Figure 2.1 for how the CCDs are arranged. When the filters were upgraded in 2015 the other four CCDs were able to be used. This resulted in the images having 36 CCDs for the first half of OSSOS and 40 CCDs in the second half. The first half was taken from 2013-2014 and the second half from 2015-2016. A single CCD is 2048 x 4612 pixels, giving MegaCam a resolution of 0.187 arcseconds per pixel.

2.1 Blocks

The sky area that OSSOS covers is split up into multiple blocks, where a block is a group of tightly packed images that creates an almost uninterrupted sky patch. Since the cameras footprint on the sky is different for the first half of OSSOS compared with the second, images are arranged differently in blocks in the first half compared with the second. The blocks in the first half contain 21 images arranged three high (along the Dec axis) and seven long (along the RA axis). The three high by one long 'columns' are offset from one another so that block runs parallel to the ecliptic. The blocks in the second half contain 20 images arranged four high and five long. The images are positioned such that the 'ears' are interlocking. Figure 2.2 contains the image layout of both the first and second half blocks.

A vast majority of the images in the first half blocks were taken in 2013/14 and a majority of the images in the second half blocks in 2015/16. Each half contains 4 blocks. The names of the first half blocks are E, O, L and H. The second half blocks are referred to as M, P D and S. The RA pointings of all the blocks are shown in Figure 2.3. Each block covers about

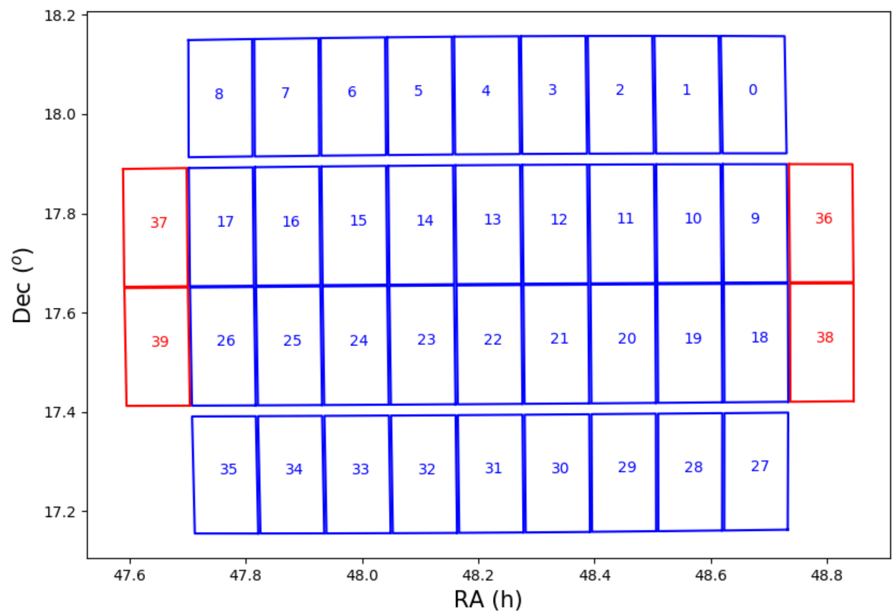

Figure 2.1: The layout of MegaCams CCDs. Each rectangle is the border of a single CCD and the CCD number is in the middle of the CCD. The blue CCDs make up the original layout and the red CCDs are the add on 'ears'.

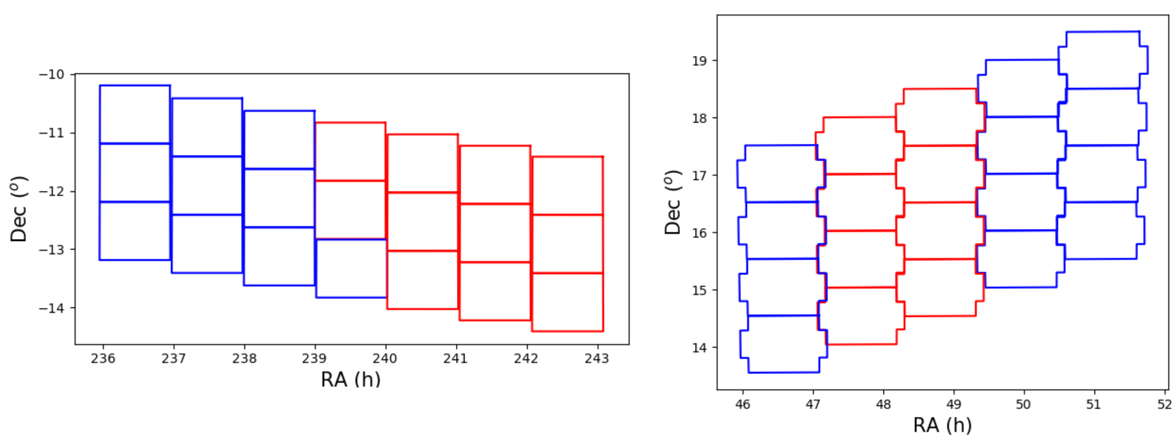

Figure 2.2: Example of the image configuration for a block in the first half of OSSOS (left) and the second half (right). The first half block is O Block and the second half block is D Block. The images that are coloured blue are from the first night of the block acquisition and red for the second.

21 square degrees[3], except L Block, which covers 20 square degrees. Giving OSSOS a total sky area of about 167 square degrees. All the blocks lie within 15 degrees of the ecliptic, and most are within 5 deg of the ecliptic[4].

The blocks were not stationary, they slowly moved parallel to the ecliptic at a speed that a typical KBO would move at. This is to minimise the number of TNOs that move out of the sky area, which goes back to the main purpose of OSSOS; to discover and track Kuiper Belt objects. This slow advance of the blocks over a semester amounts to about 0.7 degrees of the total east-west motion, meaning that only a small fraction of the block at the RA extremities have only partial repeat coverage and may have fewer observations over the course of a semester, but even there nearly all RA/Dec locations on the triples (see below) have coverage for at least half the 5-month semester.

2.2 Cadence

The cadence is split up into two parts: the triple images and the nailing images. The triple images are described in Section 2.2.1 and the nailing images are described in Section2.2.2. For much more detail about the OSSOS cadence planning, see Bannister et al. (2016).

2.2.1 Triples

Three images taken in roughly hourly intervals make up the triple. Since the exposure time of each image is five minutes, and the readout time is a minute, only 10 images can be taken in an hour. To have hourly spacings between two images of the same field, the triples for a block has to be done in two chunks of 10-11 triples each, which can be seen in Figure 2.2.

The original purpose of the triple was to discover the TNOs by looking for linear motion objects across the three images. Due to the importance of the triple, they were taken on nights that had better than average seeing. At CFHT this results in the triples often having Full Width Haft Maximums (FWHMs) in the range of 0.5-0.75″. Because OSSOS and the work in this thesis require a TNO to be detected in all three triple images, it is the worst of the three images that determines the depth for moving object detection. Luckily image quality across the OSSOS triples was very uniform (rarely more than 0.15″ change between the 3 images of the triples).

2.2.2 Nails

The nails, or nailing images, were taken at certain time differences before and after the triple images. For almost all the blocks there is at least one nail that is taken within ± 2 days of the triple, at least one ± a week, one ± a month, two ± two months. In some cases there is a nail that is ± three months from the triple. There are also nails that were taken ± a year from the triples, during the previous/next opposition.

[3]Because images with the 'ears' were slightly more than one square degree, only 20 images were needed for second half blocks to get to 21 square degrees

[4]O, H, and M blocks were placed more than 5 degrees from the ecliptic to probe the TNO inclination distribution.

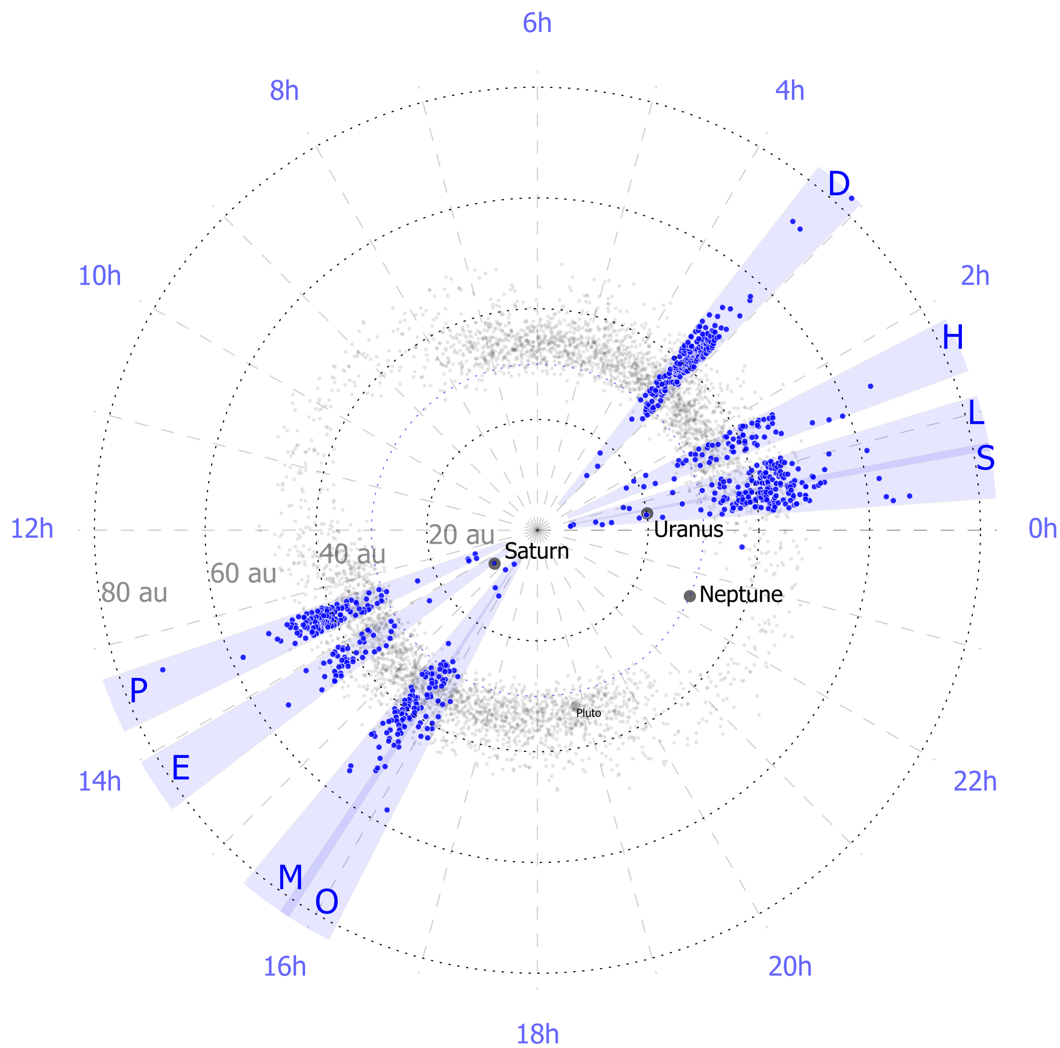

Figure 2.3: The RA pointings of all 8 OSSOS blocks. The blue dots represent the position where a TNO was discovered by OSSOS. The most distant detection, which was in D block, was at 82 au although in principle OSSOS could detect motions to at least 200 au (and 300 au in the better-seeing blocks).

The original purpose of the nailing images was to track the TNOs discovered in the triple, to be able to constrain the TNOs orbits to a high precision. Once detected in the triples the motion of the TNO could be predicted with good precision for the few nights duration out to the ±2 days nailing image, and be unambiguously identified by comparing that nail with the triple images. Once nailed to that image, successive prediction in an iterative manner to the week and months time scale was performed. For the purposes of this project, the nailing images will be predominantly used with the reverse intent: objects identified as stationary over the 2-hour triplet time span will be verified as still present in the nails that are deep enough that the objects should be visible.

2.3 Filters

Initially all of OSSOS images were taken in the r-band using the filter 'r.MP9601'. r.MP9601 has a central wavelength of 630 nm, a bandwidth of 124 nm and a mean transmission of 82.1%. As mentioned before, in 2015 MegaCams filters were upgraded. When the switch happened OSSOS started using the new r-band filter 'r.MP9602'. r.MP9602 has a central wavelength of 640 nm, a bandwidth of 148 nm and a mean transmission of 97%. The large bandwidth and better transmission of r.MP9602 compared with r.MP9601 means that r.MP9602 can detect more photons for a given exposure time and seeing, hence can see deeper.

Three of the first half blocks used the r.MP9601 filter. The last first half block, H block, had most of the images taken using the r.MP9601 filter except a few of the nails at the end of the run. These last few nailing images used the r.MP9602 filter. Part way through the second half the filter for the nails changed to the wide filter 'gri.MP9605'. This wide filter is ∼3 times wider than the r filters, so its images are deeper than the r filters. This greater depth greatly aided object recovery in nailing images with seeing somewhat worse than that of the triples obtained. Only a small fraction of the nails of M and P blocks were taken using the wide filter. A large minority of the S block nails and almost all the nails of D block were taken using the wide filter.

2.4 Catalogues

OSSOS uses two different methods to identity sources. This is to decrease the number of false positive point sources that are found in an image. The two methods are the S-Extractor method, which uses the counts of clusters of pixel to find sources, and the wavelet method, which uses wavelet decomposition theory to find sources. For a detail explanation on how these methods work please refer to Petit et al. (2004). The sources that were found using the S-Extractor method are known as jmp sources. Named after Jean-Marc Petit, the person that wrote the code using this method. Similarly, the sources that were found using the wavelet method are known as matt sources, after the person that wrote the code using this method, Matt Holman.

All of the sources found in an image gets put into a catalogue. Because there are two source finding methods there are two catalogues for each image, the jmp and matt catalogue. A catalogue contains the x-y pixel and RA-Dec position ofthe centre of the source[5] and the sources flux, maximum pixel value, elongation.

[5]The RA-Dec position was not initially in the catalogue and had to be added later for this work

To find moving objects in the triple images, all of the sources that weren't stationary need to be found. So OSSOS had to create catalogues for the triple images. For the nailing images, all that was needed was the RA and Dec plate solution[6] to know where in the image the TNO is predicted to be. This meant that the catalogues for the nails were not initially created and had to be made for this work.

2.5 In This Work

The further a solar system object is from, the Sun the slower it's on-sky motion is (Equation 1.1). Therefore distant solar system objects should appear (near) stationary in the triples but not on the timescale of a few days to months. This means the conventional OSSOS search cannot detect these objects. The strategy for this thesis was to create a catalogue of all the stationary objects that appear in the triples and then go through the nails to find them again. Stationary objects that do not show up in the nails are the examined to determine whether they are solar system objects moving less than $0.5''$/hr (and thus beyond 300 au from the Sun).

[6] the plate solution is how the pixels in the image maps to the RA/Dec coordinate system.

3. The Searching Method

The method used to search for distant objects is broken up into three key parts. The first part is the creation of the stationary catalogue, where an algorithm identifies all the stationary objects in a mosaic image (Section 3.2). The second part is the searching for the stationary catalogue objects in the nailing images (Section 3.4). The final part is creating a list of slow moving candidates and examining images of each candidate (Section 3.6). Before getting into the details of the searching method, a description of how we were able to identify an object on two different images is given in the next section.

3.1 Matching

To be able to say whether an object is real and stationary, and later to say whether it is still there or not, one must be able to match sources between different catalogues. An idealistic view would be to say if the Right Ascension (RA, δ) and Declination (Dec, δ) of two objects on different catalogues were the same then that is a match, so they are the same object. Unfortunately the real world involves uncertainty and natural variation, so the same object would have the slightly different RA and Dec in two different catalogues. Therefore a tolerance has to be introduce and one would say two sources are the same object if the on sky separation is smaller than the tolerance. Using the general formula for angular distances on the celestial sphere, two sources would be matched if their coordinates obeyed the following inequality

$$T^2 > (\delta_1 - \delta_2)^2 + ((\alpha_1 - \alpha_2)\cos(\delta_1))^2 \tag{3.1}$$

where T is the tolerance, it given value is explain in Section 3.2.3, and the subscript 1 and 2 denote two different candidates matching sources in two images.

3.1.1 Streamlined Matching

The algorithm would have to do a significant number of matches between objects in two different catalogues if all the objects in the catalogue are checked, resulting in large computational time, going as N1*N2, with N being the number of sources in a catalogue. By only checking a fraction of the catalogues we can drastically decrease the computational time. Although this needs to be done without the risk of missing a potential match. The term matcher, which will be used below, will refer to the source in the first catalogue that sources in the second catalogue will be tried to be matched to. Matchee will refer to a source in the second catalogue.

By sorting a catalogue by increasing declination we can guess where in the catalogue the possible matches are. The index, I, of where in the matchee catalogue the declination are similar to that of the matcher, assuming the increase in declination is constant, is found using

$$I = \frac{\delta - \delta_{min}}{\delta_{max} - \delta_{min}} l \tag{3.2}$$

where δ is the declination of the matcher, δ_{min} and δ_{max} are the minimum and maximum declination respectively in the matchee catalogue, and l is the length of the matchee catalogue. To find an appropriate starting position I is reduced by $0.01l$ (A hundredth of the length of the matchee catalogue) until the following inequality is true

$$\delta_I < \delta - T \tag{3.3}$$

where δ_I is the declination of the Ith object in the matchee catalogue and T is the appropriate tolerance (see Section 3.2.3). Once the inequality is satisfied the algorithm preforms a matching check on all the objects in the catalogue sequentially from the Ith object until this inequality is met

$$\delta_I > \delta + T \tag{3.4}$$

Essentially the algorithm checks all the objects in the catalogue with a declination in the range of plus or minus the tolerance from the matchers declination. This streamlined matching method is used for all the catalogue matches in the algorithm and results in more than an order of magnitude faster execution.

3.2 Creating the Stationary Catalogue

The stationary catalogue is a list of the objects that appear to be stationary, within tolerances, over the two hours in which the triple images were taken. First we find stationary objects using the jmp and matt catalogue separately: we create a jmp stationary catalogue and a matt stationary catalogue, see Section 3.2.1. Then we combine the jmp and matt stationary catalogue to create a final stationary catalogue, see Section 3.2.2.

3.2.1 jmp and matt Stationary Catalogues

An algorithm is used to created the jmp/matt stationary catalogue using the following method. The algorithm goes through the first triple images catalougue, one source at a time, and tries to match it to sources in the other two triple image catalogues. First the second triple image catalogue (which will be known as catalogue two) is search for possible matches using the wide tolerance, see Section 3.2.3. If there are more than one catalogue two matched object, the algorithm redoes the match but with a tight tolerance, see Section 3.2.3 as well. If this tight search produces only one match, then the third triple image catalogue (which will be known as catalogue three) is searched, also using the tight tolerance. If one match is again the result, the algorithm tries to match the catalogue two matched object to the catalogue three matched object, using the tight tolerance. If that match is successful then these three sources are considered a stationary object and added to the stationary catalogue. These stationary objects found with the tight tolerance are given the status of 'immune', which is useful later, see Section 3.2.4.

If no stationary object was found using the tight tolerance or if there was only one catalogue two matched object using the wide tolerance, then the algorithm searches catalogue three using the wide tolerance. If one or more catalogue three matched objects were found, the algorithm tries to match the catalogue two matched object (the ones that were found using the wide tolerance) to the catalogue three matched object, using the wide tolerance.

3.2.2 Final Stationary Catalogue

The final stationary catalogue is the intersection of the jmp and matt stationary catalogues. Therefore to make it into the stationary catalogue we require it to be found in both the jmp and matt catalogue on all three triple images. This is to cut down on non-real objects getting in the final stationary catalogue. To create the final stationary catalogue we matched the jmp stationary catalogue with the matt stationary catalogue using tolerances given in Section 3.2.3. The average position in all three triple images is used as the position of a jmp/matt stationary catalogue object in the matching. This final stationary catalogue will, from now on, be known as the stationary catalogue.

3.2.3 Tolerances

The tolerances we want to use needs to take into account two factors. The first factor is the uncertainty in the position of sources due to the source being blurred by the atmosphere. The second factor is the movements of our targets. If we want to search for objects as close as 300 au then distance traveled by the objects at the inner edge becomes non-negligible in the time frame of the triple. The wide tolerance for stationary catalogue creation is calculated by summing the angular distance a body traveling at 0.5 arcseconds per hour would cover between the two images and the average of the image seeings

$$T_w = \beta\sqrt{S_{Tx}^2 + S_{Ty}^2} + 0.5t_{xy} \tag{3.5}$$

where S_{Tx} and S_{Ty} are the seeings of the two triple images, β is a tolerance coefficient and t_{xy} is the time between the two triple images. The difference in Julian date between two images, in units of hours, is used as t_{xy}. If the two seeing were the same, we wanted the seeing part of the wide tolerance to be equal to the seeing. So we decided on a beta value of $\frac{1}{\sqrt{2}}$. Just the seeing part of the wide tolerance is used for the cases where a tighter tolerance is needed

$$T_t = \beta\sqrt{S_{Tx}^2 + S_{Ty}^2} \tag{3.6}$$

The same β value used for the wide tolerance is also used for the tight tolerance.

When matching the jmp and matt stationary catalogue, to created the stationary catalogue, the worst seeing of the triple images is used as the tolerance. We don't have to worry about the motion of slow moving objects in the tolerance since the objects position is averaged over the three images.

3.2.4 Crowding

If there are a, b and c sources that are all within the tolerance from each other in first, second and third triple image respectively, then the code will $a \cdot b \cdot c$ stationary objects. One of the ways were tried to fix this multiplicity problem was to do the tight search. This helped when there was a real object in the sources, but not if it is just a bunch of rubbish sources.

The next way we tried to solve the multiplicity problem was to remove the duplicates in the stationary catalogue. We went through each object in the stationary catalogue, from lowest to highest Dec, and tried to match it with other objects in the stationary catalogue. The sum of the worst seeing of the three triple images and the angular distance a body traveling at 0.5 arcseconds per hour would cover between the two images was used as the tolerance

```
48.1314007699 14.8073824444 48.1314006186 48.1314047704 48.1313985996 48.1314010704 48.1314031354 48.1313964252 ..
.. 14.8073975145 14.8073712102 14.8073695923 14.8074052414 14.8073758476 14.8073752605 687.73 613.91 492.11 23294.4 ..
.. 27957.02 26740.37 3805.0 2287.72 1.16 0
48.1143399616 14.8082718238 48.1143388131 48.1143432284 48.1143445087 48.1143387823 48.1143368908 48.1143375459 ..
.. 14.8082694455 14.8082719547 14.808270203 14.8082725373 14.8082693815 14.808277421 136.27 127.11 109.45 5586.02 ..
.. 5632.82 5234.16 1973.0 456.51 1.22 0
48.1727496004 14.8086946687 48.1727493395 48.1727473581 48.1727507883 48.1727466923 48.1727478864 48.1727555377 ..
.. 14.8086948694 14.8086945154 14.808694109 14.8086953876 14.8086945146 14.8086946161 33777.65 32575.2 33308.2 ..
.. 2441686.0 2475728.0 2492010.0 65097.0 63253.8 1.06 0
48.1393181221 14.8088762082 48.1393133338 48.1393078427 48.1393303148 48.1392989591 48.139324379 48.1393339032 ..
.. 14.8088817573 14.8088797403 14.8088635259 14.8088894937 14.8088673644 14.8088753675 82.25 78.65 70.85 5891.88 ..
.. 4966.62 3925.74 1709.0 182.2 1.39 0
...
```

Table 3.1: Example of a stationary catalogue file.

$$T = S_{Tw} + 0.5t_{xy} \tag{3.7}$$

where S_{Tw} is the worst seeing of the three triple images. If there is a match, the object with the higher declination is removed from stationary catalogue, unless it is 'immune'. Since objects found using the tight tolerance are most likely real objects, we do not remove them. If an object gets matched to an 'immune' object, nothing happens. Later when that 'immune' object gets rematched with the first object, then the first object gets removed from the stationary catalogue. Each object in the stationary catalogue gets a number called 'multi', which is the number of other objects it removed. Even though this value is recorded it is not used.

3.2.5 Stationary Catalogue format

The stationary catalogue is a text file were each line represents a stationary object. The first column is the averaged RA value of all six catalogues, and the second column is the average DEC value. The next six columns are the six RA values from each catalogue, the first three are from the jmp catalogues and the last three are from the matt catalogues. Each set of three is in chronological order. Similarly the next six columns are the Dec values, and the six after that are the flux values. The next column is the median jmp 'Max Int' value and the column after is the median matt value. The next column is the median jmp elongation, and the last column is the *multi* which is described in Section 3.2.4. See Table 3.1 for an example of the stationary catalogue file.

3.3 Parameters

Before the nailing catalogues can be searched, some information about the nails and the triple has to be obtained. An important piece of information about the nails is the RA and Dec range that each CCD covers, so we know which nailing catalogues we need to search in since the nailing images are at constantly moving pointing each night. Unfortunately the area of sky that the CCD cover are not rectangles with sides being constant in either RA or Dec, so it is difficult to know the exact sky area of a CCD. To solve this problem we use two boxes to describe each CCD: An inner box and an outer box. The sides of the boxes are constant in either RA or Dec. All of the inner box is in the CCD sky area and all of the CCD sky area is within the outer box, see Figure 3.1. Therefore if an object is within the inner box then it is definitely in the CCD sky area. If an object is outside the inner box but inside the outer box then the object might be in the CCD sky area, and a further check is required. Lastly, if the

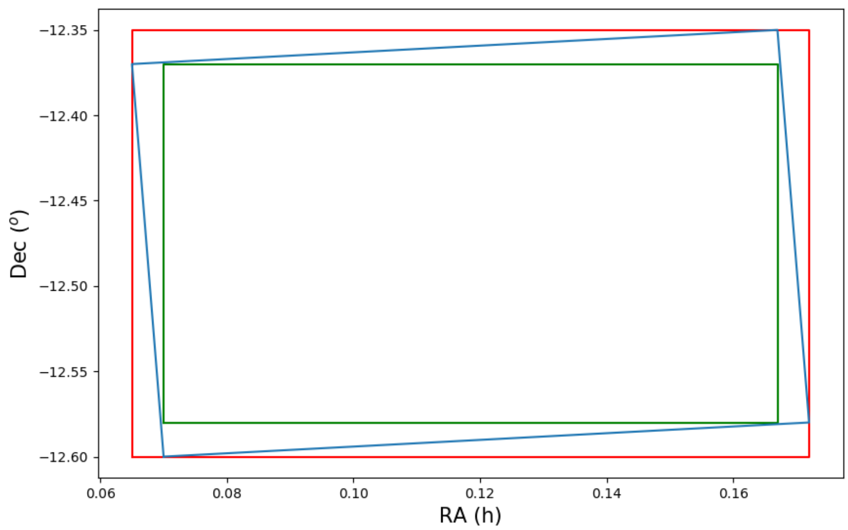

Figure 3.1: An example of the inner/outer box method used. The blue box represents the area covered by the CCD, the green box is the inner box and the red box is the outer box. This is not a real area covered by a CCD, the amount of rotation of the CCD sky area is accentuated.

object is outside the outer box then the object is not in the CCDs sky area.

The boxes are created by first finding the RA and DEC of CCDs corner pixels. The larger of the bottom two corners Dec is the Dec of the bottom side of the inner box, and the smaller Dec is the Dec of the bottom side of the outer box. Similarly, the smaller/larger of the top two corners DEC is the Dec of the top side of the inner/outer box. This process is repeated to find the RA of the left and right sides of the boxes.

For a particular nailing mosaic image, the largest and smallest RA and DEC values obtained from the sky areas of the mosaics CCDs are recorded to create a box containing all the sky area of the mosaic image. This box will be known as the nailing box.

Other information that is required is the seeing and zero point of each CCD, the exposure time of the image, the filter used, and the date which the image was taken. All of these are extracted from the image headers.

All of these nailing image parameters are put into a single text file. The file is formatted such that each nailing image has its own line with the first column being the images odometer number. The next four columns are the minimum and maximum, RA and Dec that describes the nailing box coordinates (min RA, max RA, min Dec, max Dec). The following two columns are the filter used and the exposure time of the image. The last column is the Julian date of when the image was taken rounded down to the nearest day.

Below each nailing image line in the file is a line for each of the CCDs of that image. The first column of a CCD line is the ccd number. The next four columns are the minimum and

```
1828172 49.087339 50.335460 15.787888 16.789221 gri.MP9605 300.133000 57245
ccd00 50.111982 50.218112 16.552550 16.788323 50.109115 50.221323 16.552491 16.788899 3700 5183 4.48 33.608000
ccd01 49.998254 50.105395 16.552437 16.788828 49.995716 50.108274 16.552305 16.789083 3638 5128 4.46 33.604000
ccd02 49.884006 49.991984 16.552367 16.789159 49.881861 49.994467 16.552079 16.789190 3631 5596 4.40 33.610000
ccd03 49.769556 49.878051 16.552127 16.788773 49.767662 49.880281 16.551551 16.789221 3773 5545 4.34 33.558000
ccd04 49.654921 49.763975 16.551453 16.788007 49.653473 49.765759 16.550777 16.788685 3850 5532 4.23 33.624000
ccd05 49.540504 49.649637 16.550663 16.786874 49.539230 49.651250 16.549775 16.787895 4162 5829 4.05 33.548000
ccd06 49.426179 49.535508 16.549741 16.785452 49.425382 49.536647 16.548616 16.786840 4110 5997 4.17 33.589000
ccd07 49.312483 49.421649 16.548466 16.783615 49.311985 49.422494 16.547197 16.785277 4296 6062 4.06 33.625000
ccd08 49.199419 49.308266 16.547289 16.781659 49.199301 49.308736 16.545802 16.783667 3915 5895 4.26 33.535000
...
```

Table 3.2: Example of a nailing parameters text file.

maximum, RA and Dec that describes the outer box coordinates (min RA, max RA, min Dec, max Dec). Similarly the following four columns are for the inner box. The next two columns is the length of the jmp and matt catalogue respectively. The final two columns is the CCDs seeing and zero point respectively. For an example of a nailing parameter file see Table 3.2.

Some additional information about the triples is also needed, To if a nail overlaps with the triple, the sky area of each triple is calculated the same way as the nails. A box, known as the triple box, that spans the lowest to highest RA and DEC of the triple mosaic images is created.

3.4 Searching the Nails

Once the nailing parameters file is created, the nailing images can be searched for the appearances of each object in the stationary catalogue. Initially the code loaded all the nailing catalogues for the block in question. When it was time to run the code on blocks with a higher number of nailing images the code failed due to memory issues. This was remedied by only loading the nailing catalogues of use for the stationary catalogue being examined. A nailing catalogue was consider useful if the sky area of the image it belonged to overlapped with the sky area of the triple image being examined. The nailing box, see Section 3.3, is used as the boundary of the nails sky area and likewise the triple box is used as the boundary of the triples sky area.

3.4.1 On Pixels

The algorithm goes through each nailing image to see if the stationary catalogue object is in one of its nailing catalogues. To start with the algorithm checks to see if the sky position of the stationary object might be on a nailing image. If the stationary object lies within the image box, the object might be on one of the CCDs, so it looks at each individual CCD of the image. If the stationary object does not lie within the image box, the next nailing image is checked.

A CCDs inner and outer box is used to determine if the sky position of the stationary object is on the CCD. If the coordinate position lies in the inner box then the stationary object is considered *on pixels*. If the coordinate position lies outside the inner box but inside the outer box then the RA and Dec position is converted into x and y pixel position of the nailing image. If the xy pixel position corresponds an actual pixel on the image then the stationary object is considered on pixels. If the coordinate position lies outside the outer box then the stationary object is not on pixels.

When the algorithm finds that the stationary object is on pixels on a nailing image it searches through the catalogue of that nailing image to find if a source is present at the expected RA and Dec. The searching method is outlined in Section 3.1 and the matching tolerance used is outlined below.

3.4.2 Tolerance

When matching between the stationary catalogue and a nailing catalogue the following tolerance is used

$$T = \beta\sqrt{S_T^2 + S_N^2} \tag{3.8}$$

where S_T is the seeing of the worst triple image, S_N is the seeing of the nailing image and β is the tolerance coefficient. Just like in Section 3.2.3, a value of $\frac{1}{\sqrt{2}}$ is used for β.

If there is a match then the stationary object is considered *found* in that nail. Once a match has been found the algorithm stops searching through that catalogue and searches for the next nail. Both the jmp and matt catalogues are searched.

3.5 Creating the Master Table

Once the nails have been searched, the information is recorded in a text file known as the master table. The master table contains all the stationary catalogue of a single image, along with all the nailing images each stationary object should be on pixels and whether they were found on a particular nail. Below is a description of exactly what is in the master table and how it is organised.

Each stationary object has one line in the master table that contains information about the triple images that they are in. These lines are called the stationary object lines. The first column of the stationary object lines is the objects unique identifier. The identifier is the odometer number of the first triple image the stationary catalogue object appears on followed by a dot, then the CCD number and finally the objects position in the stationary catalogue. For example, if stationary catalogue object is on CCD05 of the triple image 1755517 and is the 234th image on the stationary catalogue then its identifier would be 175517.050234.

The next six columns is the objects six RA values in the triple images. Then followed by the six DEC values, the six flux values. The next two columns are the median jmp and matt 'max int' values respectively. The 'max int' values are to do with the maximum pixel value of the source. The jmp elongation value is the following column[7] The next two columns are the maximum seeing and zero point of the triple images. The last two columns contain the exposer time and the filter used.

Below each stationary catalogue line is information about the nailing images that they are on pixels. There is one line for each nailing image that the object is considered on pixels. All nailing lines contain the following information: the nails odometer number, which CCD the object is/should be on, filter used, exposure time, seeing, and the zero point. If the object was found in the jmp and/or matt catalogue, then there is additional information. The first

[7]The 'max int' and elongation values were, at one point, going to be used. We decided that they were not needed but they were kept in the master table.

```
1846160.111542 47.953081 47.953143 47.953212 47.953096 47.953151 47.953187 14.709081 14.709001 14.709043 14.709083 ..
.. 14.709043 14.709058 50.30 54.65 54.93 1858.34 1270.47 1141.97 1595.00 78.10 1.51 0 3.06 32.740 400.32 r.MP9602
1828216 ccd00 gri.MP9605 300.18 5.39 33.519 matt 47.953133 14.709048
1828217 ccd00 gri.MP9605 300.17 5.41 33.562
1831712 ccd00 gri.MP9605 300.12 3.90 33.540 jmp 47.953091 14.709021
1832621 ccd39 gri.MP9605 300.14 3.26 33.424 jmp 47.953140 14.709042 matt 47.953144 14.708960
1836410 ccd25 gri.MP9605 450.15 3.86 33.973 jmp 47.953148 14.709024 matt 47.953136 14.709010
1836589 ccd15 gri.MP9605 450.17 4.46 34.054 matt 47.953106 14.709005
1846610 ccd10 gri.MP9605 450.32 3.53 33.890 jmp 47.953259 14.709067
1847469 ccd09 gri.MP9605 450.19 3.22 33.969 jmp 47.953167 14.709029 matt 47.953175 14.709036
1847477 ccd09 gri.MP9605 450.18 3.36 33.987 jmp 47.953194 14.709087 matt 47.953167 14.709085
1850927 ccd25 gri.MP9605 450.16 3.29 33.943 jmp 47.953163 14.709047 matt 47.953156 14.709062
1850964 ccd25 gri.MP9605 450.08 7.25 33.864
1852577 ccd23 gri.MP9605 450.17 3.08 34.060 jmp 47.953125 14.709010 matt 47.953129 14.709016
1852587 ccd23 gri.MP9605 450.17 3.09 34.062 jmp 47.953152 14.709094 matt 47.953148 14.709089
```

Table 3.3: Example of a master table.

additional column is either 'jmp' or 'matt'. Indicating which catalogue the object was found on. Followed by the RA and DEC of the object on the nail. There could be up to two of these sets of additional columns, one for jmp and one for matt. For an example of a master table see Table 3.3.

3.6 Vetting

A decision has to be made which stationary catalogue objects could be slow moving solar system objects by how many nails they reappear in. Section 3.6.1 below details the criterion a stationary catalogue object has to meet in order to be slow moving candidate. The format for the candidate list is contained in Section 3.6.2. Section 3.6.3 explains how the candidates are examined further to determine whether they are slow moving objects.

3.6.1 Candidate List

As mentioned in Section 2.2.1 the triple images have, on average, better seeing than the nailing images. Therefore an object that is at the limit of detectability in the triple images might be too faint to be seen in the worst seeing nails. This may cause some of the faint stationary objects that are actually stars and are to faint to be seen in the nails to be incorrectly labeled as a slow moving candidate.

The way we determine the flux that separate bright and faint objects is by looking at the average number of *founds* for binned jmp flux values. Assuming that a majority of objects in the stationary catalogue are real, the average number of *founds* for a particular flux bin should not depend on flux if the objects are bright enough to be seen on all the nails. The consistency of the average number of founds for bright flux is evident in Figure 3.2. When looking at the low flux end, the objects are too faint to be seen in all the nails. The average number of *founds* for the low flux bins should, therefore, be less than the average number of *founds* of the high flux bins, which can also be seen in Figure 3.2. The flux at which the average number of *founds* starts to drop is used as the dividing line between bright and faint objects.

If an object was too faint to be seen in a nail then that nail should not be counted as being *on pixels* for that nail. Therefore a way to determine the quality of the nailing image compared

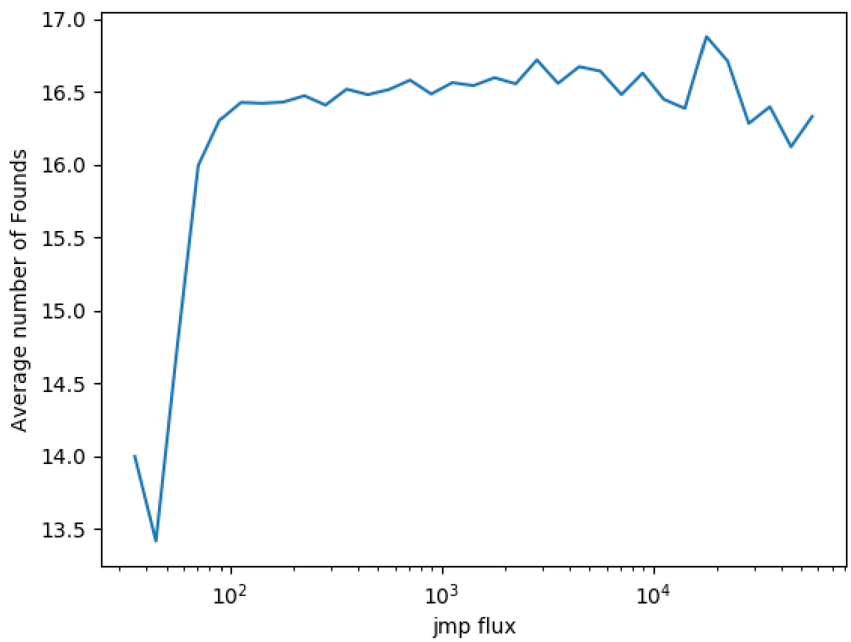

Figure 3.2: The average number of *founds* for logirithmicaly spaced binned jmp flux values. The drop off at low fluxes is due to these objects being to faint to be seen on the worst nails. The point at which the fluxes start to drop off is used as the dividing line between faint and bright objects. This figure was created using data form P block.

to the triple images was devised. If a faint object was not found on the nail, in either the jmp or matt catalogue, then an image quality check is performed. The first check is to see whether the seeing of the nail is worse than that of the triple

$$S_N > S_T + 0.25 \tag{3.9}$$

The seeings are in number of pixels. As can be seen by the equation above, the nails seeing was allowed to be slightly worse than that of the triple. If the nail does pass the first check, Equation 3.9, then a second check is performed. This time to use the zero points

$$S_N > \sqrt{2.5^{\Delta Z_p}} S_T \tag{3.10}$$

where ΔZ_p is the difference between the zero point of the nail and the triple. If the second inequality is also satisfied, then the nail is deemed not deep enough to see the faint object in question and the nail is not counted as being on pixels for that object.

Generally a wider band will means more photons from the source being detected, resulting in the image being deeper. The cut above does not take this into account, this cut only works if the filters used for both the triple and the nail have the same band. The two red filters have the same band, but the wide filter doesn't, therefore a different cut is needed when the dealing with nails using the wide filter (since the triples are always using one of the two r band filters). The wide filter is three times wider than the r band filter, so if an objects colour is approximated to being grey then the wide filter will receive three times as many photons per second from the object compared with the red filters. If the nailing image was taken using the wide filter then the following inequality

$$S_N > \sqrt{3 \frac{t_N}{t_T}} S_T \tag{3.11}$$

is used to determine whether the nail should be considered, where t_N is the exposure time of the nailing image and t_T is the exposure time of a single triple image. If the inequality is met then the nail is deemed not deep enough to see the faint object in question and the nail is not counted as being on pixels for that object. Since it is assumed that bright objects should be seen on all the nails, they do not undergo a quality check.

Ideally a slow moving object would be a stationary catalogue object that doesn't have any *founds*. There is a chance that an asteroid, a cosmic ray, noise etc. could happen to create a source where the slow moving object was, resulting in a false *found*. Therefore stationary catalogue objects with a couple of *founds* should be looked at as well. We decided that faint objects that have two or less *founds* should be considered a candidate. Since there are less of them and, if they are really stars, they have a higher chance of being *found*, bright objects that have three or less *founds* should be considered a candidate.

Due to the shifting of the nails night by night, some stationary objects on the edge of the block may only have only a couple of nails which they are on pixels. Therefore if criteria for being a candidate only depends on the number of *founds*, there will be objects that only have a few on pixel nails and are *found* on all/most of them that make it to the candidate list. To stop these kind of objects getting into the candidate list, the on pixel count must be 5 or more to be considered a candidate.

```
3
1845955.000699 47.008786 14.439502 1845955p00 1845967p00 1845993p00 1828216p08 1828217p08 1831712p08 1832625p08 ..
.. 1836414p05 1846188p00 1847469p07 1847477p07 1850931p05 1852581p03 1852591p03
1845955.001150 47.057304 14.510514 1845955p00 1845967p00 1845993p00 1828216p08 1828217p08 1831712p08 1832625p07 ..
.. 1836414p06 1846188p00 1846610p10 1847469p07 1847477p07 1850931p05 1852581p02 1852591p02
1845955.010761 46.900652 14.451291 1845955p01 1845967p01 1845993p01 1828216p08 1828217p08 1831712p08 1832625p08 ..
.. 1836414p06 1846188p01 1847469p10 1847477p10 1850931p06 1852581p05 1852591p05
1845955.020016 46.850212 14.321343 1845955p02 1845967p02 1845993p02 1831712p08 1832625p08 1836414p06 1836583p06 ..
.. 1836593p06 1836595p06 1836597p06 1847446p00 1847461p00 1850931p05 1852581p03 1852591p03
1845955.020194 46.850105 14.351472 1845955p02 1845967p02 1845993p02 1831712p08 1832625p08 1836414p06 1836583p06 ..
.. 1836593p06 1836595p06 1836597p06 1847446p00 1847461p00 1850931p05 1852581p03 1852591p03
..
```

Table 3.4: Example of a candidate list file.

By examining objects that have on pixel count of 5 or more, we exclude a few percent of the total object. To reduce the number of objects excluded we make some exceptions. If an object has an on pixel count of 4 and is found on 1 or fewer of them or on pixel count of 3 and no founds then that object is a candidate. This means that, by also examining objects that only have 4 or 3 on pixel nails, less than a percent of objects are excluded from examination.

3.6.2 Candidate List format

The candidate list contains the stationary sources unique identifier followed by its average RA and DEC position. The next three columns are the image names of the three triple images (in chronological order). An image name is the odometer number of the image followed by a *p* then the CCD number. The remaining columns contain the image names of all the nails that the candidate is on pixels. The first row only has the number 3 in it (which is explained in the section below). The candidate list filename is the odometer of the first triple image followed by '.vetting'. For an example of a candidate list see Table 3.4.

3.6.3 Validate

To determine whether or not the objects in the candidate list are slow moving objects the images were viewed. This was achieved using a programme called validate[8]. Validate uses the information in the candidate list file to display cut outs of given images centred on inputted coordinates. The RA and Dec (second and third column respectively) of the file is used as the input coordinates and following image names are the given images. Validate displays one cut out at a time and a button has to be clicked in order to view the next (or previous) cut out in the sequence. There is also an accept and a reject button. Once the candidate is accepted or rejected then images of next candidate pop up. If a candidate is accepted a comment can be added.

There are two rounds of image viewing. The first round only the triple images are viewed. This is to quickly remove all the candidates that are not point sources, like artifacts from bright star halos. The 3 in the first row of the candidate list is to tell the software that only the first three images (triples) should be viewed. The candidates that were accepted in the first round of vetting were placed into another candidate file. This new candidate list didn't have a 3 in its first line, therefore allowing all images to be viewed. From viewing the nails, one can determine whether the object is slow moving in the outer solar system.

[8]validate was written by JJ Kavelaars at the Hertzberg Research Institute

4. Results

After applying the method described in Chapter 3 to each image in each block, we found no distant solar system object. The number of candidates for each square degree ranged from 10s to a couple of hundred. Almost all of the stationary objects that make it into the candidate list are false positive. The main types of false positive candidates are described in Section 4.1.

Even though no distant solar system object was found, we did find some objects that weren't false positives. They include optical ghosts of very bright stars (Section 4.2), what we believe are faint flare stars (Section 4.4) and faint supernovae (Section 4.3).

4.1 False Positive

There are four main types of false positives. The two most common are cause by saturated star halos (Section 4.1.1) and faint stars (Section 4.1.2). Other types of false positives that are less frequent, and thus not discussed, are chance alignment of noise, stars right next to galaxies, galaxies on the edge of a CCD.

4.1.1 Saturated Stars Halo

Saturated stars produce a 'halo' around themselves that produce enormous numbers of sources in each triple catalogue. Since the telescope comes back to nearly the same sky patch for the triples, a saturated star appears on nearly the same part of the triple images, so its halo has nearly the same shape. This results in chance alignments of halo-produced sources that the code thinks is are stationary objects, because they are within tolerances of being at constant RA and Dec. In the nails, the saturated star will be in a different part of the image, so its halo will have a different shape. The halo-produced sources will not line up with the halo created stationary objects. The halo-created stationary objects will have no *founds* and thus be labeled as a candidate.

These kinds of false positives are easy to reject. By looking at just the triple images, one can tell they are not point sources, hence cannot be solar system objects. Therefore they can be quickly rejected in the first vetting pass.

4.1.2 Faint Stars

As discussed earlier, stars that are near the flux limit in the triples may not be visible in the worst seeing nails. Therefore some of these faint stars may only have a couple of good seeing nails resulting in one or two *on pixel* nails and thus being placed in the candidate list. These are real object but are false in the sense that they are not moving.

We attempted to stop these faint stars from showing up in the candidate list by not counting the nails that were 'worse' that the triples (see 3.6.1) but it apears to be not 100% successful. Identifying stationary objects as faint stars was the most time consuming part of examining the candidate lists, although the process was made easier, and occurred less often, when there were nails taken using the wide filter.

4.1.3 Obscured Stars

Some bright stars also make it into the candidate list when a star is partly or fully covered up by a diffraction spike from a saturated star almost all of the *on pixel* nailing images. This covering up of the star causes the source finding software to be unable to detect it. So the star 'appears' in only in a couple of nails. These false positives can be quickly rejected in the second vetting pass.

4.1.4 Inbetween Stars

There are a group of false positive that appear in the space between two close stars but there is nothing at the given coordinates. They are believed to be created when two stars close to each other are matched together and create a false stationary object between the two. These false positives only appeared in the second half blocks, for reasons unknown.

For the first two blocks they were found, candidates that were this kind of false positive were accepted in the first round of vetting then rejected in the second. To save time they were rejected in the first round of vetting for the remaining blocks. The order is irrelevant because the are clearly not moving objects.

4.2 Optical Ghosts

Optical Ghosts are internal reflections of very bright stars that appear to be slowly moving in the triples. Since the block is slowly shifting, explained in Section 2.1, when the telescope comes back for the next triple image the field has slightly shifted, resulting in the optical ghost moving a tiny amount, but less that the stationary tolerance in the triples. When it comes to the nails, the block has shifted enough that the optical ghost is no longer anywhere near its position in the triples. The movement of an optical ghost can be seen in Figure 4.1. The last three images make up the triple and the first image is a nail taken 2 months before.

The total number of optical ghosts found was 26. Even though they are technically false positives, their similarities to slow moving solar system objects warrant a discussion about them. The similarities were so close that the first optical ghost found was initially thought to be a slow moving solar system object.

The way to differentiate between an optical ghost and a slow moving solar system object is to closely examine the object's movement. On the timescale of a few hours, solar system objects have linear speeds. Optical ghosts, on the other hand, appear to have a slight change in direction and speed. Another telltale sign that an object is an optical ghost is the direction of the movement. Mentioned in Section 1.4.1, the on-sky motion of objects out beyond a few hundred au are dominated by Earths orbital velocity. So much so that bound objects at that

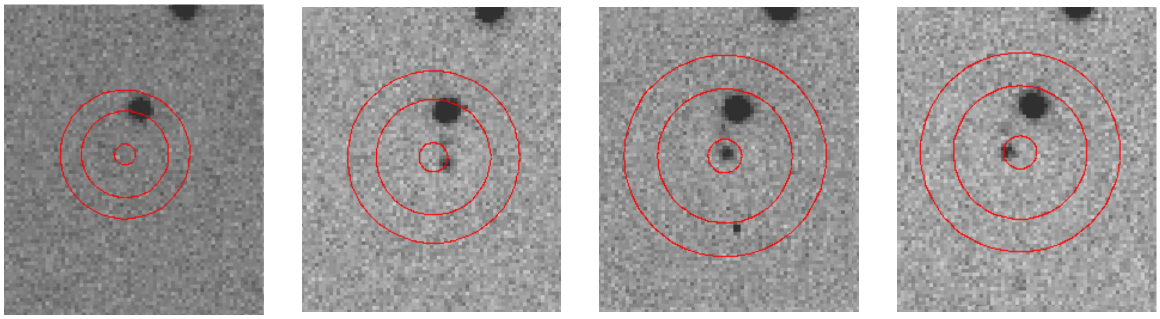

(a) 2 months before. (b) First triple image. (c) Second triple image. (d) Third triple image.

Figure 4.1: The movement of an optical ghost in the triples and one nail (others not shown) to show the ghost is not in the vicinity in the nailing images. These images are from E Block.

distance all have the same direction on the sky, parallel with the ecliptic. Therefore if an object is not traveling in this direction it is not a (bound) solar system object.

4.3 Supernovae

The code was able to find distant supernovae. They were supernova that had their peak brightness around the time of the triples and were faint enough that they could only be spotted in a few of the nails. One of the supernova that was found is shown in Figure 4.2. It appears the brightest in the triples images and the nail the day after with nothing in the nails before. In the nail a month later the supernova has dimmed but still visible but in the nail 8 months later it can no longer be seen. A rapid rise time of less that a week and then fading over several weeks is typical of supernova light curves. Additionally, the supernovae were all seen in the outskirts of galaxies, as one would expect. The total number supernovae found was 34.

It is most likely that there are more supernovae in the data that didn't make it into the candidate list due supernovae reappearing on too many nails. If there is scientific interest the code could be altered to extract additional supernovae, but without multi color follow-up when they were visible, there is little scientific value.

4.4 Possible Flare-Star Pheomena

A phenomena similar to supernova was also discovered in the list of candidates. They were point sources that were visible in all three triples and in the nails a few days either side of the triple but nothing in any of the other nails. What differs these objects from supernovae is that there are no galaxies close by and nothing could be seen in the nails that were a week or a month later. We suspect that they might be flare stars that are normally below the magnitude limit and flare up around the time of the triples.

The rise times of flares tend to be tens to hundreds and the decay times (from max luminosity to half of it) is minutes to hours. These timescales are correlated with the flare energy(Pettersen, 1989). Thus, the presence of signal 'days later but not weeks later' is more in line with a flare

[9]The two nailing images that the supernova was found on were the two nails that were taken the day after the triple. The supernova in the nail one month after was not detected even though it can be clearly seen.

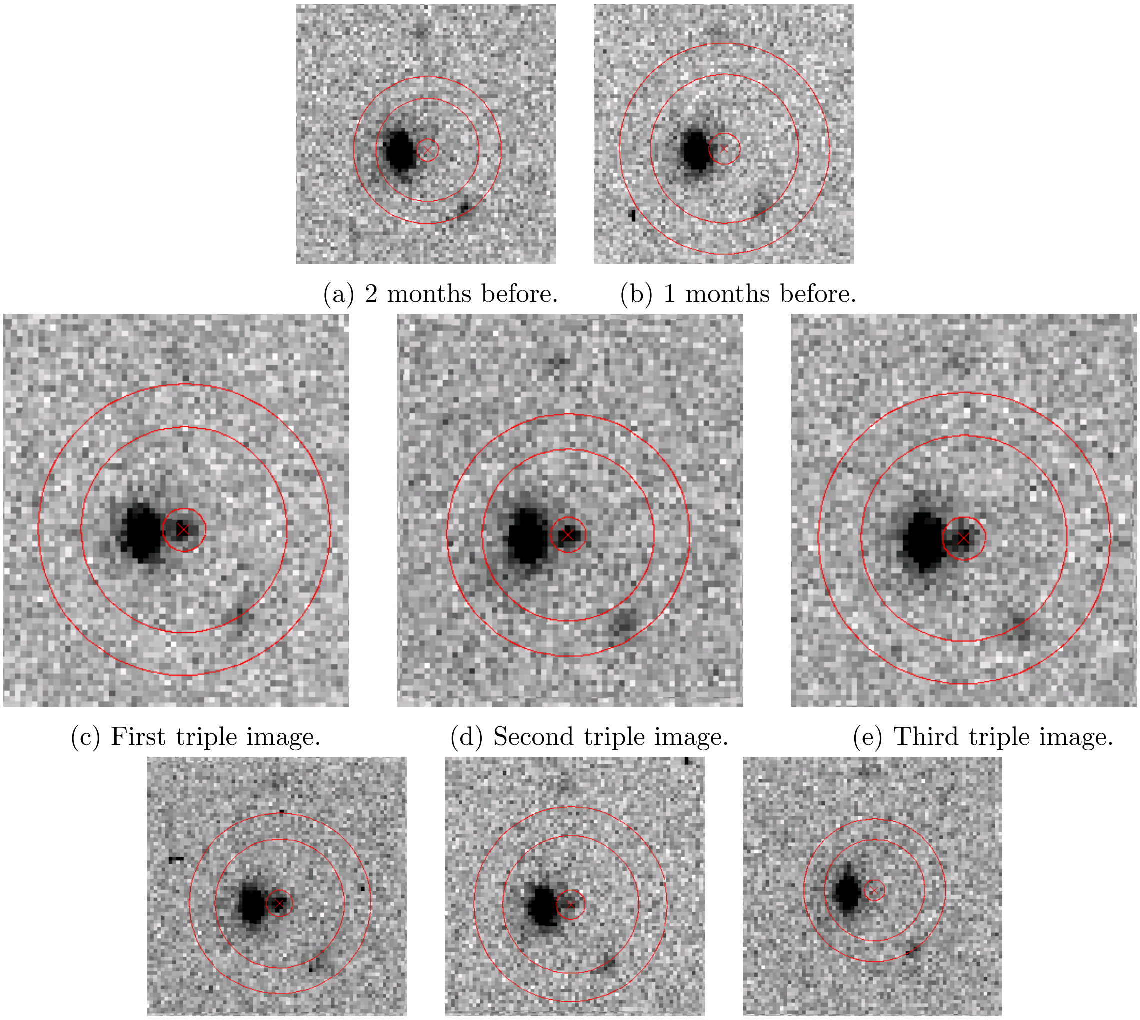

(a) 2 months before.
(b) 1 months before.
(c) First triple image.
(d) Second triple image.
(e) Third triple image.
(f) A day after.
(g) 1 month after.
(h) 8 months after.

Figure 4.2: Images of a supernova event captured by OSSOS and labeled as a solar moving solar system candidate by our code, because it was only detected by the code on two nailing images[9]. The supernova occurs in the centre of the red circles with its host galaxy on its left. These images are from L Block.

star then with a supernovae, but most flare stars decay on time scales of hours rather than days. Because these were never detected in the wings of galaxies it may be more likely to be energetic flares from stars in the halo of our galaxy, but these events will be on the energetic end of known flare phenomena. While there may be interest in exploring this in future work, these are clearly not moving objects and thus were not pursued in this thesis. The total number of these flare-stars-like objects found was 32.

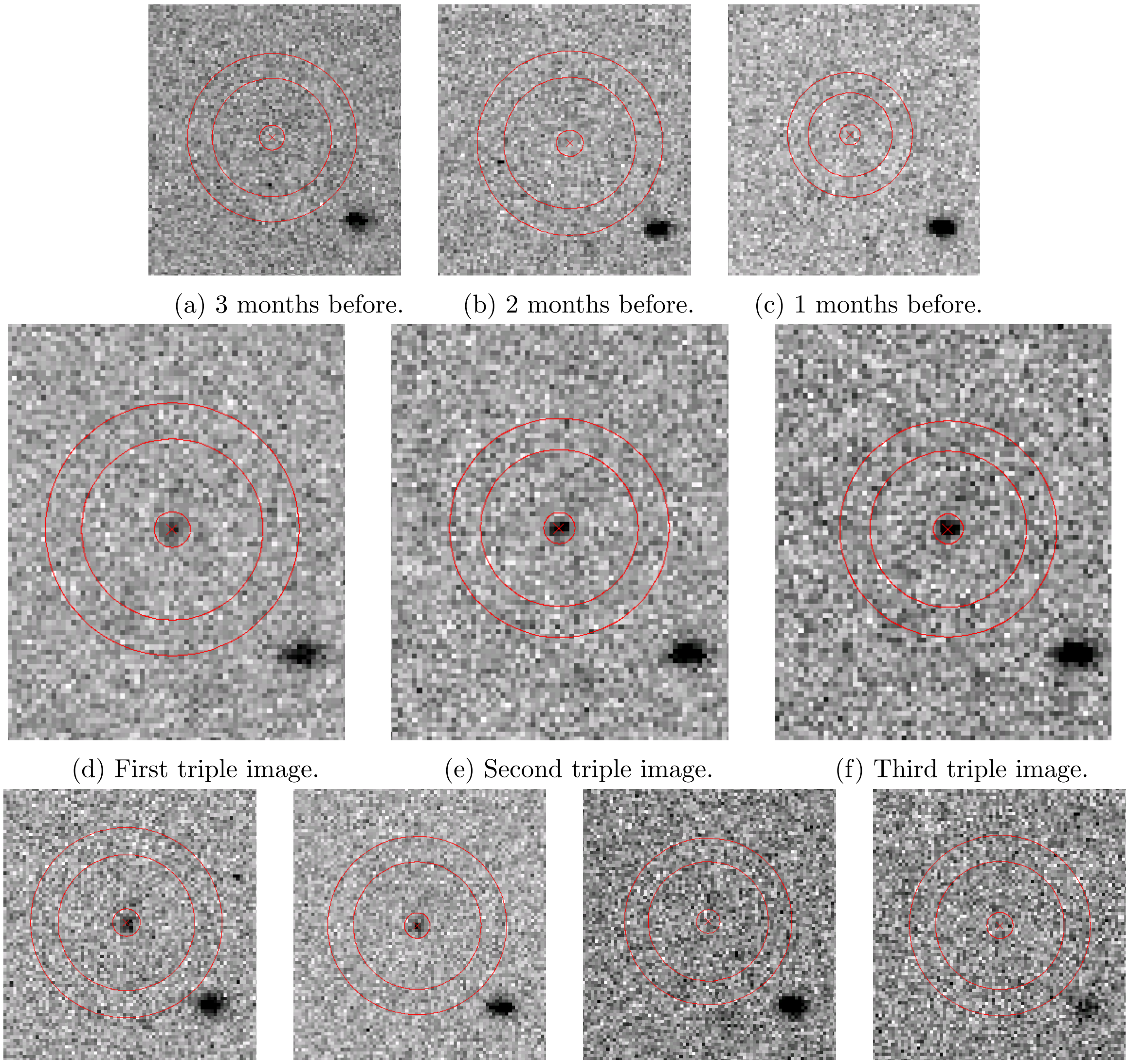

(a) 3 months before. (b) 2 months before. (c) 1 months before.

(d) First triple image. (e) Second triple image. (f) Third triple image.

(g) A day after. (h) 3 days after. (i) 1 months after. (j) 3 months after.

Figure 4.3: Images of what is believed to be a flare star captured by OSSOS and labeled as a solar moving solar system candidate by our code. These images are from P Block.

5. Constraints on Distant Planets

Even though no solar system object was discovered, we can use this null result to place an upper limit on the number of the largest TNOs in the outer solar system. To get an upper limit we need to make some assumptions. Firstly we assume that the code would have found a real solar system object if one was there since some of the objects that made it into the candidate list behaved similarly to a slow moving solar system object, especially the optical ghosts (Section 4.2). Therefore no planting and finding of artificial objects was required to establish a magnitude detection limit. Secondly we assume that the efficiency of the code to find a real solar system object of a certain r magnitude is the same as that established for OSSOS(Bannister et al., 2016). From this assumption the survey simulator used for OSSOS can be used for this work too.

Section 5.1 details how the survey simulator works and the distributions used for this work. The statistics of the simulated objects we are able to detect is given in Section 5.2. Finally, Section 5.3 details how we use the survey simulator to produce an upper limit to the number of the largest TNOs in the outer solar system.

5.1 Survey Simulator

A survey simulator was created for OSSOS to bias a postulated orbital model to compare to that found by OSSOS (see Kavelaars et al. (2009) for a description). The simulator works by creating one object at a time from an input orbital and size distribution and assessing whether this object would have been found by OSSOS. For every OSSOS triple image the simulator calculates the objects sky position at the time the image was taken to see if the object is in the images field of view. If the object is in an images field of view the simulator probabilistically determines if it is found based on its calculated apparent magnitude and sky motion. The sample of simulated detections from this model can be compared to those found by OSSOS. If they are not similar then the input distribution is not a correct representation of the actual distribution. The simulator can also be used to estimate the number of intrinsic objects there must be in order to acquire a certain number of detections.

5.1.1 Orbital Distribution

The orbital distribution used for this work consists of a uniform a (see Section 1.2) ranging from 150 au to 999 au. For the pericentre distribution we assume that it is also uniformly distributed starting from 33 au, just outside the orbit of Neptune, out to 99 au. The eccentricities are calculated using e = 1 - q/a. The inclination distribution we use is the typical $\sin i$ times a Gaussian. Since SOs and DOs are part of the hot TNO population we use a width of 13° with the minimum and maximum values being 0 and 180° respectively. All the other parameters, longitude of the ascending node, the argument of pericentre and the mean anomaly, are uniformly distributed from 0 to 360°.

Mag range	No. of Objects	Fraction with r < 21.3	Fraction with d < 300 au
-3 < H < -2	1862	0.38	0.42
-2 ≤ H < -1	1990	0.33	0.54
-1 ≤ H < 0	2088	0.30	0.72
0 ≤ H < 1	2104	0.28	0.98
1 ≤ H < 2	1956	0.26	1.00
Total sample	10000	0.30	0.72

Table 5.1: The simulated sample of 10,000 objects that OSSOS (extended by our analysis out to >1000 au) would detect, broken down into absolute magnitude bins. See text for discussion.

5.1.2 Size Distribution

For the simulated size distribution we wanted to examine objects ranging from smallest object that we would have been able to detected up to a Mars sized object. A Mars sized object (with a Pluto albedo) would have an absolute magnitude of -3. The smallest object that we can detect would have an apparent mag of 25.5 at 300 au. This corresponds to an object with a $H_r \approx 0.7$, which in the visual is $H_v \approx 1.2$. The matching tolerance used in making the stationary catalogue (Section 3.2.3) allowed the algorithm to find objects moving slightly faster than 0.5″/hour, due to the seeing of the triples. The closest object the algorithm deployed in this thesis could detect was actually slightly closer than 300 au. Due to this, and the fact the range would be a convenient 5 magnitudes, we decided to simulate down to H = 2 objects. $\Delta 5$ mags corresponds to a change in radius by a factor of 10. Therefore the H mag range we used was -3 to 2.

For the slope of the size distribution, we use the current size distribution of known TNOs (see Figure 1.4 as a reference). Since the largest H value in our range, H = 2, is lower than the apparent knee between slopes at H ∼ 3, the simulated sample will be situated in size region where the size distribution slope is shallow, $\alpha = 0.14$. Because of this, and that there is no reason to believe the slope changes for TNOs larger than Pluto, we used a logarithmic size distribution with a slope of $\alpha = 0.14$ for the entire simulated population.

5.2 Large Sample

To get a better understanding of the detectability of our synthetic distributions we ran the survey simulator was until 10,000 objects were detected from the orbital and H-magnitude distributions just described. We split the simulated sample up into five groups of equal H mag ranges. The H mag ranges for each group can be seen in Table 5.1 along with the number of objects in each group. As can be seen there is rough the same number of objects in each group, due to the shallow absolute magnitude distribution which results in small objects not vastly outnumbering the larger ones.

When looking at the cumulative fraction of the objects distance at detection, Figure 5.1, one can see that, even though all the objects come within 100 au, most of them are detected at distances of > 100 au. Therefore a survey needs to be sensitive to sub arcsecond per hour speeds to be able to detect a large portion of these objects. Another obvious feature is differences between the different H mag groups. The groups with a lower H were detected at larger distances. Almost all of the $1 \leq H < 2$ group being detected within 300 au, thus would not

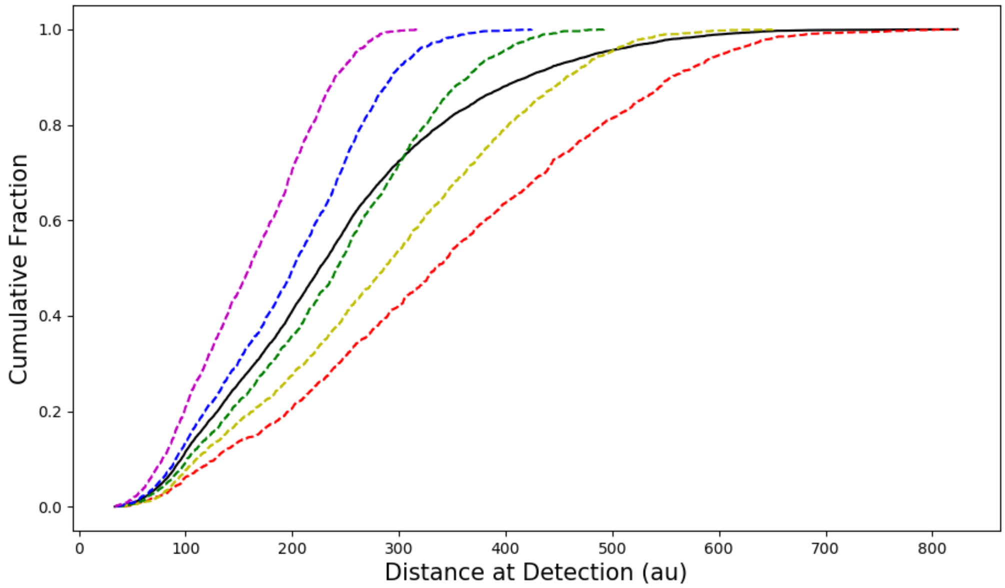

Figure 5.1: The cumulative fraction of the heliocentric distance the simulated objects were at time of detection. The black solid line represents the total sample of 10,000 objects. The coloured dashed lines represent different H magnitude range: red for -3 < H < -2, yellow for -2 ≤ H < -1, green for -1 ≤ H < 0, blue for 0 ≤ H < 1 and magenta for 1 ≤ H < 2. Even the smallest objects are in majority detected beyond 100 au and thus require sensitivity to <1″/hr rates.

have been detected by this work but rather the original OSSOS reduction which was sensitive to rates faster than 0.5″/hr. In contrast, more than half of the -3 < H < -2 group (Mars scale) would be detected beyond 300 au. Table 5.1 contains the fraction of objects found within 300 au for each group and the total sample. For the total sample 0.72 of the objects were detected within 300 au. Therefore the main part of OSSOS had a better chance of finding high-a TNOs compared to this work.

The cumulative distribution of 'apparent magnitude at detection' is shown in Figure 5.2. One can see that there is little difference between the different H mag groups. The higher H mag groups have a slightly higher fraction for a given r mag compared with the lower H mag groups. If OSSOS had a r mag limit that was the same as the Schwamb and Brown survey limit of 21.3 (Section 1.4.2), only 0.3 of the simulated objects would have been detected. That value goes down to 0.26 for the smallest objects and up to 0.42 for the largest objects, see Table 5.1. Even though a Schwamb and Brown mag limit would have detected only 30% of the objects OSSOS would have detected per unit area, Schwamb and Brown had ∼70 times more sky area that OSSOS. Thus, as an overall search, that survey will outperform OSSOS, but is unable to detect faint and/or very distant objects.

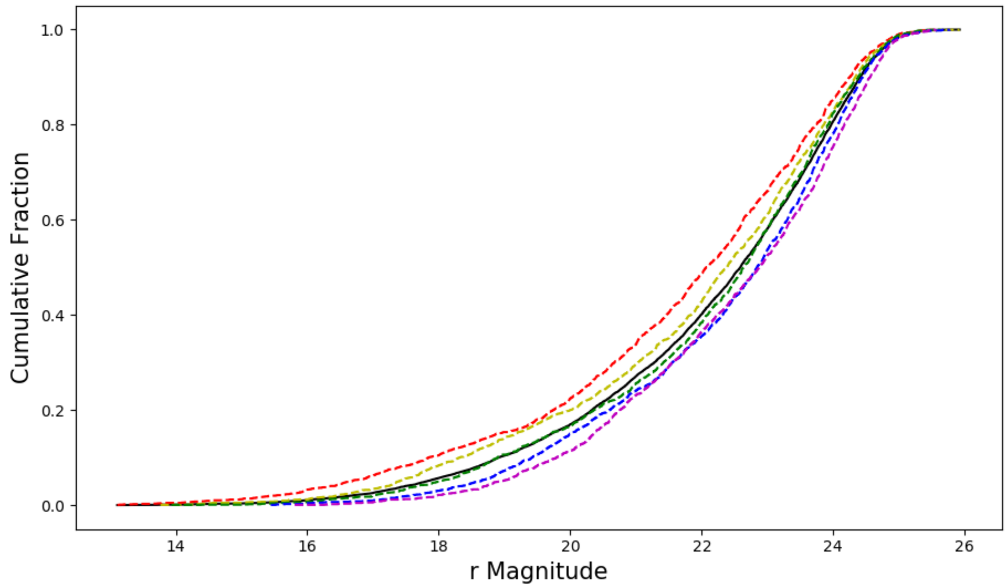

Figure 5.2: The cumulative fraction of the r magnitude of the simulated objects at time of detection. The black solid line represents the total sample of 10,000 objects. The coloured dashed lines represent different H magnitude range: red for -3 < H < -2, yellow for -2 $\leq$ H < -1, green for -1 $\leq$ H < 0, blue for 0 $\leq$ H < 1 and magenta for 1 $\leq$ H < 2.

To examine what part of the orbit, in terms of distance from the Sun, the objects were when detected we create a quantity known as the fractional orbital distance, which is defined by

$$F = \frac{d - q}{Q - q} \tag{5.1}$$

where d is the heliocentric distance to the object when they would be detected, q is the pericentre and Q is the apocentre of the object. When $d = q$ then $F = 0$ and when $d = Q$ then $F = 1$. We compared the distribution of F for 3 different magnitude ranges (-3 < H < -2, -1 $\leq$ H < 0, 1 $\leq$ H < 2) by putting F into 15 bins, seen in Figure 5.3. The smallest objects are predominantly found at lower F values, near pericentre, whereas the largest objects were more uniformly spread with a spike at apocentre. This makes sense since the larger objects can be detected further out, see Figure 5.4. These further out objects will be closer to apocentre, where Kepler's 2nd Law indicates they spend more time (and if detected there, they contribute a spike of signal). In contrast, the fainter objects are in vast majority only visible near perihelion.

5.3 Upper Limit of Dwarf Planets in the Outer Solar System.

If we expect to get 3 detections then the Poisson likelihood of getting no detections is $e^{-3} \simeq 5\%$. Therefore the OSSOS null detection allows us to say the number of intrinsic model objects that must be checked before obtaining 3 simulated detections thus serves as an estimate of the 95% upper limit on the true intrinsic population of these large objects. We ran the simulator until we got 100 values for the upper limit[10]. A histogram of the 100 trials of this calculation (using

[10]since the simulator runs until 3 objects are tracked there were simulations where an object was detected and not tracked. This resulted in the simulator stopping at the 4th detected object (3rd tracked object).

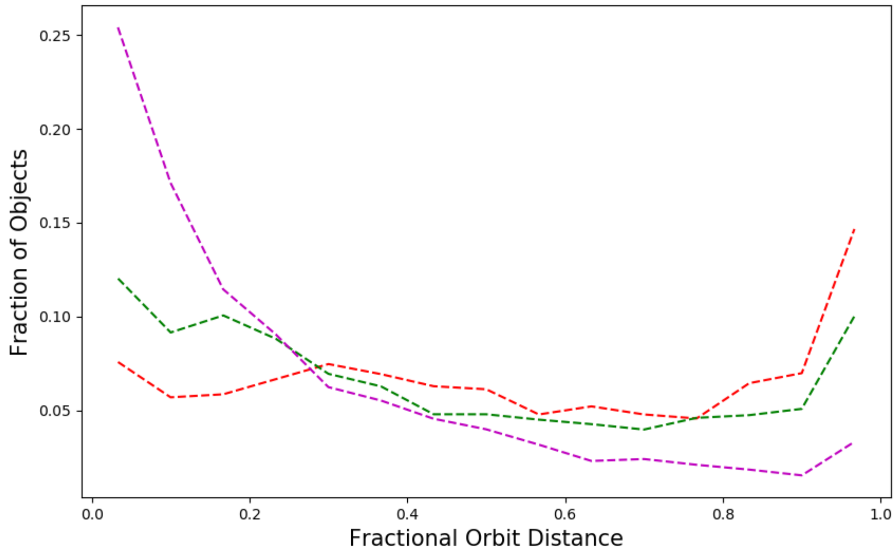

Figure 5.3: The fraction of objects with a certain fractional orbital distance for different H magnitude ranges: red for -3 < H < -2, green for -1 ≤ H < 0 and magenta for 1 ≤ H < 2. Each group has around 2000 values which are split up into 15 bins. Note that all semi-major axes are represented here, allowing a few of the physically smallest objects (magenta-coded) objects to be detectable near apocentre.

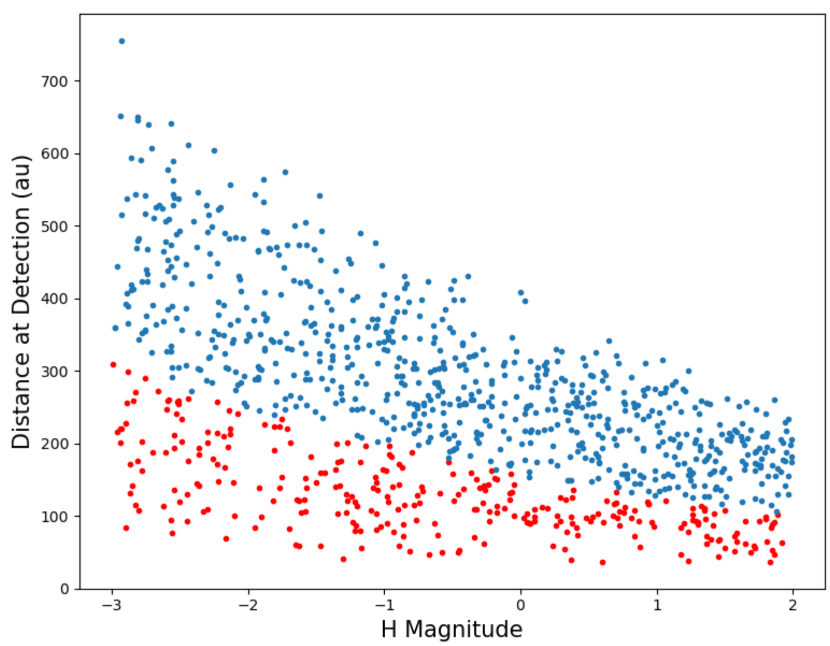

Figure 5.4: A plot of the first 1000 objects in the simulated sample. Red represents an r mag of less than 21.3 and blue represents a r mag of greater than 21.3.

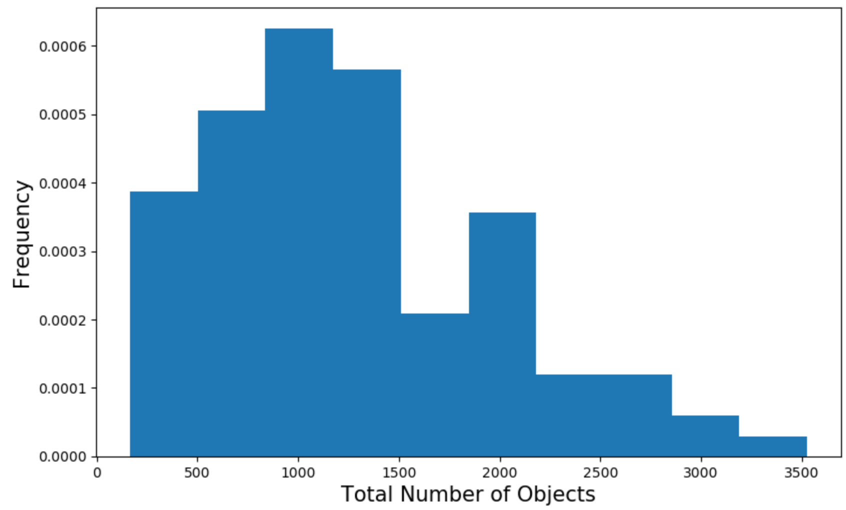

Figure 5.5: A histogram of the intrinsic population of simulated objects when the three of these objects are detected.

different random seeds for the object-generation algorithm) is shown in Figure 5.5. The sample has a median value of 1145. The range that encompasses 95% of the values, centred on the median, is 286 to 2876. Therefore we estimate that the 95% upper limit to the number of dwarf planets in the outer solar system is 1100^{+1700}_{-800}.

6. Conclusion and Future Work

After searching through the ∼160 square degrees of OSSOS for a slow moving object beyond 300 au, 34 supernovae, 32 possible flare stars and 26 optical ghost were found but no solar system objects. By simulating high semi-major axis SOs and DOs we obtained an understanding of statistics of the objects we were sensitive to. By finding the total number of simulated objects needed to get 3 detection we were able to state the 95% upper limit on the number of dwarf planets (-3 > H > 2) in this scattering and detached orbit population, of 1100^{+1700}_{-800}.

Although this work is the first search sensitive to Mars-scale objects at 500-1000 au, the upper limit of $\sim$ 1000 objects from $-3 < H < 2$ is not very constraining. The half of this distribution ($H < -0.5$) corresponds to Pluto-scale and larger objects, and estimates based on the fact the 3 such objects (Pluto, Eris, and Triton) are currently known have been used (e.g. Nesvorný and Vokrouhlický (2016)) to estimate that $\sim 1000 - 4000$ must have existed in the very early Solar System during the planetary migration phase, given an estimated 'retention efficiency' of order 10^{-3}. Thus, a *current* upper limit of 1000 such bodies is not very constraining to these late-stage planetary formation models as those models would indicate likely <10 such objects remain in the outer reaches of our Solar System.

When thinking about future surveys to find the largest members still lurking in the large-a population, the main factor is the slope of the size distribution. The fact that the slope in the region of the largest TNOs is so shallow means that it is better to increase the sky coverage compared to depth. Therefore to maximise the likelihood of finding a large distant object, a future survey should reduce the magnitude limit to be all-sky. However because we are dealing with such a small number of objects that are dwarf planet size, it may be that all the of the currently-exisiting objects are fainter than the all-sky magnitude limit, resulting in no detections (like the Schwamb and Brown survey). If no there were no detections the next step would be to increase the magnitude limit and look at patches of the sky, having in mind that the elusive object may simply be where one is not looking.

A future survey that has the most promise of finding a distant solar system object is the upcoming Large Synoptic Survey Telescope (LSST). LSST is an 8.4m diameter all-sky survey telescope that will search for transient objects like TNOs. It will be able to detect objects down to about magnitude 24.5, and have multi-night sensitivity allowing the lowest rates to be detected. The main data flow will include hunting for outer solar system moving objects (https://www.lsst.org/science/solar-system/oss). Chapter 5 showed that given the OSSOS sky coverage and magnitude depth, it would detect of order 0.3% of the intrinsic population. The sky coverage of LSST will be about 9000 square degrees, that is ∼60 times the size of OSSOS. Since LSST and OSSOS have a similar mag depth then LSST should have a $sim20\%$ chance of finding a $H < 2$ distant outer solar system object. Thus, even if there remains only 10 dwarf-planet and larger scale objects in the distant solar system, LSST should detect a couple. Because LSST will be nearly all-sky, doing much better after LSST's survey will require all-sky synoptic coverage to deeper than 25th or 26th magnitude; there are no current plans for any facilities with that capability.

Bibliography

Agnor, C. B. and Hamilton, D. P. (2006). Neptune's capture of its moon Triton in a binary-planet gravitational encounter. *Nature*, 441:192–194.

Bannister, M. T., Kavelaars, J. J., Petit, J.-M., Gladman, B. J., Gwyn, S. D. J., Chen, Y.-T., Volk, K., Alexandersen, M., Benecchi, S. D., Delsanti, A., Fraser, W. C., Granvik, M., Grundy, W. M., Guilbert-Lepoutre, A., Hestroffer, D., Ip, W.-H., Jakubik, M., Jones, R. L., Kaib, N., Kavelaars, C. F., Lacerda, P., Lawler, S., Lehner, M. J., Lin, H. W., Lister, T., Lykawka, P. S., Monty, S., Marsset, M., Murray-Clay, R., Noll, K. S., Parker, A., Pike, R. E., Rousselot, P., Rusk, D., Schwamb, M. E., Shankman, C., Sicardy, B., Vernazza, P., and Wang, S.-Y. (2016). The Outer Solar System Origins Survey. I. Design and First-quarter Discoveries. *The Astronomical Journal*, 152:70.

Batygin, K. and Brown, M. E. (2016). Evidence for a Distant Giant Planet in the Solar System. *The Astronomical Journal*, 151:22.

Boss, A. P. (1997). Giant planet formation by gravitational instability. *Science*, 276:1836–1839.

Brown, M. E. (2001). The Inclination Distribution of the Kuiper Belt. *The Astronomical Journal*, 121:2804–2814.

Kavelaars, J. J., Jones, R. L., Gladman, B. J., Petit, J.-M., Parker, J. W., Van Laerhoven, C., Nicholson, P., Rousselot, P., Scholl, H., Mousis, O., Marsden, B., Benavidez, P., Bieryla, A., Campo Bagatin, A., Doressoundiram, A., Margot, J. L., Murray, I., and Veillet, C. (2009). The Canada-France Ecliptic Plane Survey - L3 Data Release: The Orbital Structure of the Kuiper Belt. *The Astronomical Journal*, 137:4917–4935.

Lambrechts, M. and Johansen, A. (2012). Rapid growth of gas-giant cores by pebble accretion. *Astronomy and Astrophysics*, 544:A32.

Lawler, S. M., Shankman, C., Kaib, N., Bannister, M. T., Gladman, B., and Kavelaars, J. J. (2017). Observational Signatures of a Massive Distant Planet on the Scattering Disk. *The Astronomical Journal*, 153:33.

Lissauer, J. J., Hubickyj, O., D'Angelo, G., and Bodenheimer, P. (2009). Models of Jupiter's growth incorporating thermal and hydrodynamic constraints. *Icarus*, 199:338–350.

Luhman, K. L. (2014). A Search for a Distant Companion to the Sun with the Wide-field Infrared Survey Explorer. *The Astrophysical Journal*, 781:4.

Nesvorný, D. (2011). Young Solar System's Fifth Giant Planet? *The Astrophysical Journal*, 742:L22.

Nesvorný, D. and Vokrouhlický, D. (2016). Neptune's Orbital Migration Was Grainy, Not Smooth. *The Astrophysical Journal*, 825:94.

Petit, J.-M., Holman, M., Scholl, H., Kavelaars, J., and Gladman, B. (2004). A highly automated moving object detection package. *Monthly Notices of the Royal Astronomical Society*, 347:471–480.

Pettersen, B. R. (1989). A review of stellar flares and their characteristics. *Solar Physics*, 121:299–312.

Schwamb, M. E., Brown, M. E., and Rabinowitz, D. L. (2009). A Search for Distant Solar System Bodies in the Region of Sedna. *The Astropysical Journal*, 694:L45–L48.

Shankman, C., Kavelaars, J. J., Bannister, M. T., Gladman, B. J., Lawler, S. M., Chen, Y.-T., Jakubik, M., Kaib, N., Alexandersen, M., Gwyn, S. D. J., Petit, J.-M., and Volk, K. (2017). OSSOS. VI. Striking Biases in the Detection of Large Semimajor Axis Trans-Neptunian Objects. *The Astronomical Journal*, 154:50.

Sheppard, S. S. and Trujillo, C. (2016). New Extreme Trans-Neptunian Objects: Toward a Super-Earth in the Outer Solar System. *The Astronomical Journal*, 152:221.

Weidenschilling, S. J. (1977). Aerodynamics of solid bodies in the solar nebula. *Monthly Notices of the Royal Astronical Society*, 180:57–70.

Young, R. E., Smith, M. A., and Sobeck, C. K. (1996). Galileo Probe: In situ Observations of Jupiter's Atmosphere. *Science*, 272:837–838.